Sayı : 10059539-02035251
Konu : Olurlar, Onaylar

Bilimsel Araştırma Projeleri Koordinasyon Birimine

Bilimsel Araştırma Projeleri Koordinasyon Birimi

Yürütücülüğünü yaptığım 2021/3-33 DOSAP numaralı projeden bir adet SCI kapsamında indekslenen Q1 sınıfındaki dergide makale yayınlanmıştır. Makalenin teşekkür kısmında BAP birimine teşekkür edilmiştir. Yayın dilekçesi ve makale ekte sunulmuştur.

Gereğini bilgilerinize arz ederim.

e-imzalıdır
Prof. Dr. Ferhan TÜMER
Öğretim Üyesi

Ek:
1- Dosap 1 yayın dilekçesi (1 Sayfa)
2- 20213-33 DOSAP yayın (19 Sayfa)

T.C.
KAHRAMANMARAŞ SÜTÇÜ İMAM ÜNİVERSİTESİ
BİLİMSEL ARAŞTIRMA PROJELERİ KOORDİNASYON BİRİMİ
PROJE YAYIN DİLEKÇESİ

Proje Adı		
Benzen Sülfonamid Esaslı Yeni Konjugatların Sentezi, Karakterizasyonu ve Çeşitli Biyolojik Özelliklerinin İncelenmesi		
Proje No	**Başlama Tarihi**	**Bitiş Tarihi**
2021/3-33 DOSAP	01-09-2021	31-10-2023
Yayın Türü	**Yayın / Makele Başlığı**	
Makale	*New sulfonamide derivatives based on 1,2,3- triazoles: synthesis, in vitro biological activities and in silico studies*	
Dergi ISSN	**DOI**	**Cilt / Sayfa / Yıl**
1538-0254	https://doi.org/10.1080/07391102.2023.2222833	1 / 1 / 2023
Yayınlandıgı Dergi Kısa Ad	**Yayınlandıgı Dergi**	
Belirtilmemiş	Journal of Biomolecular Structure and Dynamics	

İLGİLİ MAKAMA

Yukarıda bilgileri verilen ilgili otomasyona girilmiş yayın bilgileri içerisinde ; *"Söz konusu çalışma/yayın/sunum/poster/bildiri/* ***KAHRAMANMARAŞ SÜTÇÜ İMAM ÜNİVERSİTESİ Bilimsel Araştırma Projeleri birimi*** *tarafından 2021/3-33 DOSAP proje numaralı "Benzen Sülfonamid Esaslı Yeni Konjugatların Sentezi, Karakterizasyonu ve Çeşitli Biyolojik Özelliklerinin İncelenmesi" konusu ile ilgili olup, ilgili birimce desteklenmiştir." ("This work is supported by the* ***Scientific Research Project Fund of KAHRAMANMARAŞ SÜTÇÜ İMAM ÜNİVERSİTESİ*** *under the project number 2021/3-33 DOSAP")* ifadesi yer almaktadır.

PROJE YÜRÜTÜCÜSÜNÜN

Ünvanı, Adı-Soyadı : Prof.Dr. Ferhan TÜMER

Tarih : 11-09-2023

İmza :

Journal of Biomolecular Structure and Dynamics

ISSN: (Print) (Online) Journal homepage: https://www.tandfonline.com/loi/tbsd20

New sulfonamide derivatives based on 1,2,3-triazoles: synthesis, *in vitro* biological activities and *in silico* studies

İrfan Şahin, Mustafa Çeşme, Özge Güngör, Fatma Betül Özgeriş, Muhammet Köse & Ferhan Tümer

To cite this article: İrfan Şahin, Mustafa Çeşme, Özge Güngör, Fatma Betül Özgeriş, Muhammet Köse & Ferhan Tümer (2023): New sulfonamide derivatives based on 1,2,3-triazoles: synthesis, *in vitro* biological activities and *in silico* studies, Journal of Biomolecular Structure and Dynamics, DOI: 10.1080/07391102.2023.2222833

To link to this article: https://doi.org/10.1080/07391102.2023.2222833

Published online: 15 Jun 2023.

JOURNAL OF BIOMOLECULAR STRUCTURE AND DYNAMICS
https://doi.org/10.1080/07391102.2023.2222833

Taylor & Francis
Taylor & Francis Group

New sulfonamide derivatives based on 1,2,3-triazoles: synthesis, *in vitro* biological activities and *in silico* studies

İrfan Şahin[a], Mustafa Çeşme[a], Özge Güngör[a], Fatma Betül Özgeriş[b], Muhammet Köse[a] and Ferhan Tümer[a]

[a]Department of Chemistry, Faculty of Sciences, Kahramanmaras Sutcu Imam University, Kahramanmaras, Turkey; [b]Department of Nutrition and Dietetics, Faculty of Health Sciences, Ataturk University, Erzurum, Turkey

Communicated by Ramaswamy H. Sarma

ABSTRACT

Eight new hybrid constructs containing a series of sulfonamide and 1,2,3-triazole units were designed and synthesized. Anticancer, antioxidant and cholinesterase activities of these hybrid structures were investigated. In our design, the Cu(I)-catalyzed click reaction between N,4-dimethyl-N-(prop-2-yn-1-yl)benzenesulfonamide (**6**) and aryl azides **8a–h** was used. Antioxidant activity values of **9f** (IC_{50}: 229.46 ± 0.001 μg/mL) and **9h** (IC_{50}: 254.32 ± 0.002 μg/mL) hybrid structures were higher than BHT (IC_{50}: 286.04 ± 0.003 μg/mL) and lower than Ascorbic acid (IC_{50}: 63.53 ± 0.001 μg/mL) and α-Tocopherol (IC_{50}: 203.21 ± 0.002 μg/mL). We determined that the cytotoxic effects of hybrid constructs **9d** (IC_{50}: 3.81 ± 0.1084 μM) and **9g** (IC_{50}: 4.317 ± 0.0367 μM) against A549 and healthy cell line (HDF) are much better than standard cisplatin (IC_{50}: 6.202 ± 0.0705 μM). It was determined that the AChE inhibitory activities of all synthesized compounds were much better than Galantamine used as a standard. In particular, **9c** (IC_{50}: 13.81 ± 0.0026 mM) had ten times better activity than the standard Galantamine (IC_{50}: 136 ± 0.008 mM). The ADMET properties of the molecules have been thoroughly examined and met the criteria for drug-like substances. They also have a high oral absorption rate, as they can effectively cross the blood–brain barrier and are easily absorbed in the gastrointestinal tract. *In vitro* experiments were confirmed by *in silico* molecular docking studies.

ARTICLE HISTORY
Received 2 February 2023
Accepted 2 June 2023

KEYWORDS
Triazole; Alzheimer; *in silico*

1. Introduction

Alzheimer's disease (AD) is the most common chronic neurodegenerative disease faced by the increasing elderly population due to prolonging the human lifespan (Bag et al., 2015). It is estimated that the number of dementia patients in the world is 50 million at present, of which 30–35 million are Alzheimer's patients. The disease's occurrence depends on genetic and environmental risk factors (Kung et al., 2001). The most significant known risk factor is age; As you age, the likelihood of disease progression increases, but it is not an inevitable part of aging. While memory initially deteriorates, attention, language, visuospatial skills, perception, and problem-solving decline. In addition, personality changes and behavioral and psychiatric symptoms (delusions, hallucinations, affective disorders, etc.) are added. Eventually, the disease progresses to loss of bodily function and, ultimately, death (Davis, 1976; Martin Prince et al., 2015). To treat Alzheimer's disease, inhibition of the enzyme acetylcholinesterase (AChE) is an important target, and AChE inhibitors are the primary drugs for treating this disease. Current AD drugs such as enzyme inhibitors donepezil, rivastigmine, and Galantamine, currently used for therapeutic purposes, provide symptomatic relief by increasing acetylcholine levels and inhibiting acetylcholinesterase (AChE). Still, they also give various side effects such as peripheral side effects, hepatotoxicity, and gastrointestinal system disorders (Luo et al., 2016; Singla & Piplani, 2016). To overcome this situation, acetylcholinesterase (AChE) and butyrylcholinesterase (BuChE) enzyme inhibition studies of new molecules should be performed. Recent studies have stated that some molecules, as newly synthesized sulfonamide derivatives, exhibit AChE inhibition at very low concentrations (Hamedi et al., 2020; Köksal et al., 2019; Turkan et al., 2018).

Cancer is a non-communicable disease and is the second leading cause of death after cardiovascular disease (Malani et al., 2017). The increased mortality in patients affected by cancer is due to the failure of traditional therapeutic tools such as radiation therapy and surgical approaches (Kamal et al., 2008). Therefore, chemotherapeutic strategies often involve the development of small molecule anticancer agents that can be administered *via* bloodstream action targeting both cancers and metastasized colonies (Liu et al., 2016; Penthala et al., 2015). Therefore, great emphasis has been placed on reliable drug evaluation based on anticancer agents. Anticancer activities of natural compounds or new organic molecules are being studied. Due to the ineffective chemotherapy caused by drug resistance in cancer treatment and the inability of many drugs to differentiate between

CONTACT Ferhan Tümer ftumer@ksu.edu.tr Department of Chemistry, Faculty of Sciences, Kahramanmaras Sutcu Imam University, 46040, Kahramanmaras, Turkey.

cancerous cells and normal cells, research studies of agents with fewer side effects continue intensively (Duan et al., 2013; Stefely et al., 2010).

Since molecules containing heteroatoms have a wide range of biological activities, they are significant in pharmaceutical chemistry. It is known that triazoles, which are heterocyclic molecules, are also important. Compounds containing 1,2,3-triazole groups in their structure have been the subject of intense research in the field of medicinal chemistry because of their high stability against strong oxidizing and reducing environments, their tendency to make hydrogen bonds, and their easy binding to biomolecular regions as they increase their solubility (Bonandi et al., 2017; Dalvie et al., 2002; Horne et al., 2004). 1,2,3-triazoles have become important building blocks in the field of drug discovery due to their unique properties, such as being stable against metabolic degradation, having the ability to form hydrogen bonds that can easily support the binding of biomolecular targets and increasing solubility (Aziz Ali, 2021). There are triazole drugs currently on the market. Cefatrizine (**1**), tazobactam (**2**), rufinamide (**3**) are some of them (Figure 1). Structural features of 1,2,3-triazole it is common for them to be used as a bioisostere in synthesizing new active molecules by mimicking different functional groups (Bonandi et al., 2017). The 1,2,3-triazole core provides a variety of pharmacophore properties, and hybrid structures are generally considered "precursor compounds" when they contain or are fused to a 1,2,3-triazole ring (Bozorov et al., 2019).

In biomedical uses, sulfonamides are well tolerated and exhibit a wide range of biological effects, including diuretic, anticancer, antithyroid, antibacterial, anti-carbon anhydrase, antidiabetic, hypoglycemia and analgesic (Bag et al., 2015; Casini et al., 2002; Genç et al., 2008; Santos et al., 2006). According to reports, sulfonamides are among the precursors of chemotherapeutic medicines and can be used to treat the symptoms of AD. These chemicals are routinely employed to prevent and treat any diseases (Kołaczek et al., 2014).

As described above, sulfonamides and triazole derivatives show very important biological properties. We know very well from our previous studies that some triazole derivatives show anticancer, AChE and BuChE inhibitory and antioxidant properties (Çot et al., 2022; 2022; Şahin et al., 2021; 2022a; 2022b).

In our study of the synthesis of diarylmethanol compounds with 1.2,3 triazole skeletons, 14 (**6a–n**) hybrids were synthesized and their anti-cancer and antioxidant properties were studied. The antioxidant activity of other compounds (**6k**) other than a compound of the triazole derivatives studied has been found to have IC50 values lower than those of trolox, the reference anti-oxidant, and these triazol derivatives have been shown to have high antioxidants activity. On the other hand, *in vitro* anti-cancer activity on the PC3 (human prostate carcinoma) cell line of the synthesized compounds was studied and the study concluded that a compound (**6e**) had the lowest IC50 value compared to the reference substance 5-FU (IC50:40.89 μM) and had a higher anticancer activity. However, one compound (6a) has been found to have very high IC50 values (IC50: 583.53 μM) and to have weak anti-cancer activity (Çot et al., 2022).

In another study, we synthesized eight (**6a–h**) azide derivatives that participated in the structure of new 1,2,3 triazols and studied their anti-cancer and antioxidant activities. All compounds except one compound (**6e**) have been shown to have more DPPH radical scavenging capacity than BHT and β-carotene standards. According to ABTS radical cutting studies, all compounds showed higher cutting activity than ascorbic acid and Trolox. The anti-cancer activity of the synthesized compounds was determined using the HeLa cell line and compared to cisplatine (IC50: 16.30 μg/mL). Compound **6a** (IC50: 49.03 μg/mL) has a moderate level of activity compared to cisplatin (Şahin et al., 2022a).

In another study, where eight new triazole compounds (**7a–h**) were synthesized that included ester groups, the compound's anti-cancer and antioxidant activities were studied. It has been determined that all synthesized compounds exhibit antioxidant activity depending on the dose. HeLa cell line was used to determine the anti-cancer activity of the compounds and compared with cisplatine (IC50: 16.30 μg/mL). It has been concluded that **7g** of the compound (IC50: 19.78 μg/mL) has close activity with cisplatin (Şahin et al., 2023a).

Given our current studies with previous studies that looked at their anti-cancer and anti-antioxidant activities by synthesizing 1,2,3 triazole derivatives comprising different pharmacophore groups, it has been observed that the compounds have high, medium and low levels of antioxidant, anticancer, AChE and BuChE inhibitor properties depending on the pharmacaphore groups and dosage they have.

The synthesis of sulfonamide-functionalized triazoles is important for the investigation of their biological activities and the development of drug-candidate compounds. In this study, we aimed to synthesize a series of 1,2,3-triazole derivatives to determine theirs *in vitro* and *in silico* properties.

In summary, considering the results of previous studies with sulfonamide and triazole derivatives, it was thought that these derivatives could have anti-cancer, antioxidant, and anticholinesterase activity, and the design and validation of compounds by silico analysis. Eight studies of the biological activity of sulfonamide and triazole-derived compounds (anti-cancer, antioxidant, and anticholinesterase)

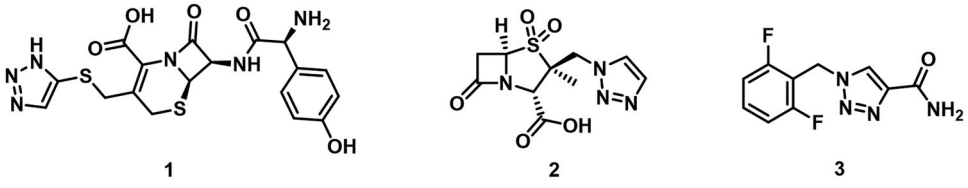

Figure 1. Triazole based drugs currently on the market.

designed with silico analyses were conducted and the results of the biological activity study with *in silico* were consistent.

2. Materials and methods

2.1. Apparatus and chemicals

All reagents and solvents were purchased from Aldrich. Costech ECS 4010 device was used for element analysis, Perkin Elmer Spectrum 400 device was used for FTIR spectra, Bruker 400 MHz NMR device was used for NMR analysis.

2.2. Synthesis of N,4-dimethylbenzenesulfonamide compound (5)

Compound **5** was synthesized according to the method given in the literature (Eggler, 1995). 4-methylbenzenesulfonyl chloride (**4**) (1 mmol) was dissolved in CH_2Cl_2 (30–40 mL) and methylamine (8.3 mmol) was added dropwise at 0 °C and stirred at the same temperature for ~2 h. The reaction progress was checked with TLC (Thin Layer Chromatography). After the reaction was complete, the solvent was removed by rotary evaporation. The substance was taken to the ethyl acetate phase and extracted with 10% $NaHCO_3$ (30 mL) solution. The organic phase was dried over Na_2SO_4, filtered and the solvent was removed on a rotary evaporator.

2.3. Synthesis of N,4-dimethyl-N-(prop-2-yn-1-yl)benzenesulfonamide compound (6)

Compound **6** was synthesized following the given literature (De Nisi et al., 2016). Compound **5** (1 mmol) was dissolved in acetone (30 mL). K_2CO_3 (2 mmol) was added to it and after it was stirred at room temperature for ~20 min, propargyl bromide (2 mmol) was added and refluxed at 85 °C overnight. The reaction progress was checked with TLC. After the starting material was completely consumed, the solvent was removed in a rotary evaporator. The material taken into the ethyl acetate phase was extracted with 1 M HCl (30 mL). The organic phase was dried over Na_2SO_4, filtered and the solvent was removed on a rotary evaporator.

2.4. Synthesis of azides (8a–h) and triazole compounds (9a–h)

Azides and triazole compounds (Figure 2) were synthesized according to the method in the literature (Şahin et al., 2021).

N,4-dimethylbenzenesulfonamide (**5**) ($C_8H_{11}NO_2S$): Yield: 92%, m.p.: 73–75 °C, colour: white, FTIR: 3261, 2979, 2923, 1314, 1306, 1153, 820. ^{1}H NMR (400 MHz, $CDCl_3$) δ 7.77 (d, $J = 8.3$ Hz, 2H), 7.34 (d, $J = 8.0$ Hz, 2H), 4.67 (d, $J = 4.8$ Hz, 1H), 2.65 (d, $J = 5.4$ Hz, 3H), 2.45 (s, 3H). ^{13}C NMR (100 MHz, $CDCl_3$) δ 143.51, 135.79, 129.74, 127.28, 29.30, 21.52. Mol. Weight = 185.1 g/mol.

N,4-dimethyl-N-(prop-2-yn-1-yl)benzenesulfonamide (**6**) ($C_{11}H_{13}NO_2S$): Yield: 92%, m.p.: 93–94 °C, colour: yellow, FTIR: 3277, 3052, 2963, 2931, 2891, 2124, 1326, 1159, 905. ^{1}H NMR (400 MHz, $CDCl_3$) δ 7.73 (d, $J = 8.2$ Hz, 2H), 7.33 (d, $J = 7.9$ Hz, 2H), 4.04 (d, $J = 2.2$ Hz, 2H), 2.84 (s, 3H), 2.45 (s, 3H), 2.10 (s, 1H). ^{13}C NMR (100 MHz, $CDCl_3$) δ 143.72, 134.17, 129.54, 127.91, 76.35, 74.00, 39.76, 34.29, 21.53. Mol. Weight = 223.2 g/mol.

N-((1-(4-methoxyphenyl)-1H-1,2,3-triazol-4-yl)methyl)-N,4-dimethylbenzenesulfonamide (**9a**): Yield: 84%, m.p.: 110–111 °C, colour: Grey, FTIR: 3127, 3004, 2840 (C-H), 1595,1519 (C = C), 1455 (N = N), 1345 (C-N), 1329 (S = O), 1256, 1230 (C-O). ^{1}H NMR (400 MHz, $CDCl_3$) δ 7.91 (s, 1H), 7.74 (d, $J = 7.9$ Hz, 2H), 7.62 (d, $J = 8.6$ Hz, 2H), 7.37 (d, $J = 7.8$ Hz, 2H), 7.04 (d, $J = 8.6$ Hz, 2H), 4.42 (s, 2H), 3.89 (s, 3H), 2.81 (s, 3H), 2.47 (s, 3H). ^{13}C NMR (100 MHz, $CDCl_3$) δ 159.95, 143.73, 134.55, 130.38, 129.83, 127.48, 127.27, 122.08, 121.28, 114.82, 55.64, 45.63, 35.04, 21.52. Anal. calcd for $C_{18}H_{20}N_4O_3S$ (%): C: 58.05; H: 5.41; N: 15.04; S, 8.61; Found (%): C: 58.01; H: 5.38; N: 15.05; S, 8.58.

N,4-dimethyl-N-((1-(p-tolyl)-1H-1,2,3-triazol-4-yl)methyl)benzenesulfonamide (**9b**): Yield: 91%, m.p.: 114–116 °C, colour: Cream, FTIR: 3127, 2922 (C-H), 1597,1517 (C = C), 1458 (N = N), 1348 (C-N), 1333 (S = O). ^{1}H NMR (400 MHz, $CDCl_3$) δ 7.94 (s, 1H), 7.74 (d, $J = 8.3$ Hz, 2H), 7.60 (d, $J = 8.4$ Hz, 2H), 7.40 – 7.32 (m, $J = 11.4$, 8.3 Hz, 4H), 4.43 (s, 2H), 2.81 (s, 3H), 2.47 (s, 3H), 2.45 (s, 3H). ^{13}C NMR (100 MHz, $CDCl_3$) δ 143.73, 139.05, 134.67, 134.60, 130.28, 129.83, 127.48, 120.37, 45.62, 35.04, 21.51, 21.09. Anal. calcd for $C_{18}H_{20}N_4O_2S$ (%): C, 60.65; H, 5.66; N, 15.72; S, 8.99; Found (%): C: 60.59; H: 5.68; N: 15.75; S, 8.95.

N-((1-(4-isopropylphenyl)-1H-1,2,3-triazol-4-yl)methyl)-N,4-dimethylbenzenesulfonamide (**9c**): Yield: 81%, m.p.: 109–110 °C, colour: Cream, FTIR: 3130, 2958, 2922, 2868 (C-H), 1599,1522 (C = C), 1462 (N = N), 1346 (C-N), 1330 (S = O). ^{1}H NMR (400 MHz, $CDCl_3$) δ 7.94 (s, 1H), 7.74 (d, $J = 8.2$ Hz, 2H), 7.63 (d, $J = 8.5$ Hz, 2H), 7.42 – 7.35 (m, $J = 9.0$ Hz, 4H), 4.43 (s, 2H), 3.07 – 2.95 (m, 1H), 2.81 (s, 3H), 2.47 (s, 3H), 1.32 (d, $J = 6.9$ Hz, 6H). ^{13}C NMR (100 MHz, $CDCl_3$) δ 150.00, 143.72, 134.84, 134.59, 129.83, 127.72, 127.48, 120.50, 45.63, 35.03, 33.84, 23.87, 21.51. Anal. calcd for $C_{20}H_{24}N_4O_2S$ (%): C, 62.48; H, 6.29; N, 14.57; S, 8.34; Found (%): C: 62.50; H: 6.25; N: 14.53; S, 8.36.

N-((1-(4-chlorophenyl)-1H-1,2,3-triazol-4-yl)methyl)-N,4-dimethylbenzenesulfonamide (**9d**): Yield: 85%, m.p.: 160–161 °C, colour: Light green, FTIR: 3118, 3065 (C-H), 1597,1501 (C = C), 1452 (N = N), 1344 (C-N), 1329 (S = O), 547 (C-Cl). ^{1}H NMR (400 MHz, $CDCl_3$) δ 8.00 (s, 1H), 7.75 (d, $J = 8.3$ Hz, 2H), 7.70 (d, $J = 8.9$ Hz, 2H), 7.54 (d, $J = 8.9$ Hz, 2H), 7.38 (d, $J = 7.9$ Hz, 2H), 4.43 (s, 2H), 2.82 (s, 3H), 2.47 (s, 3H). ^{13}C NMR (100 MHz, $CDCl_3$) δ 143.81, 135.42, 134.74, 134.55, 129.99, 129.86, 127.47, 121.62, 121.10, 45.60, 35.13, 21.53. Anal. calcd for $C_{17}H_{17}ClN_4O_2S$ (%): C, 54.18; H, 4.55; N, 14.87; S, 8.51; Found (%): C: 54.20; H: 4.50; N: 14.83; S, 8.49.

N-((1-(4-fluorophenyl)-1H-1,2,3-triazol-4-yl)methyl)-N,4-dimethylbenzenesulfonamide (**9e**): Yield: 93%, m.p.: 142–144 °C, colour: Grey, FTIR: 3122, 3069 (C-H), 1599,1513 (C = C), 1452 (N = N), 1331 (S = O), 1154 (C-F). ^{1}H NMR (400 MHz, $CDCl_3$) δ 7.98 (s, 1H), 7.77 – 7.69 (m, 4H), 7.38 (d, $J = 8.1$ Hz, 2H), 7.28 – 7.22 (m, 2H), 4.43 (s, 2H), 2.82 (s, 3H), 2.47 (s, 3H). ^{13}C NMR (100 MHz, $CDCl_3$) δ 143.79, 134.55, 129.86, 127.47,

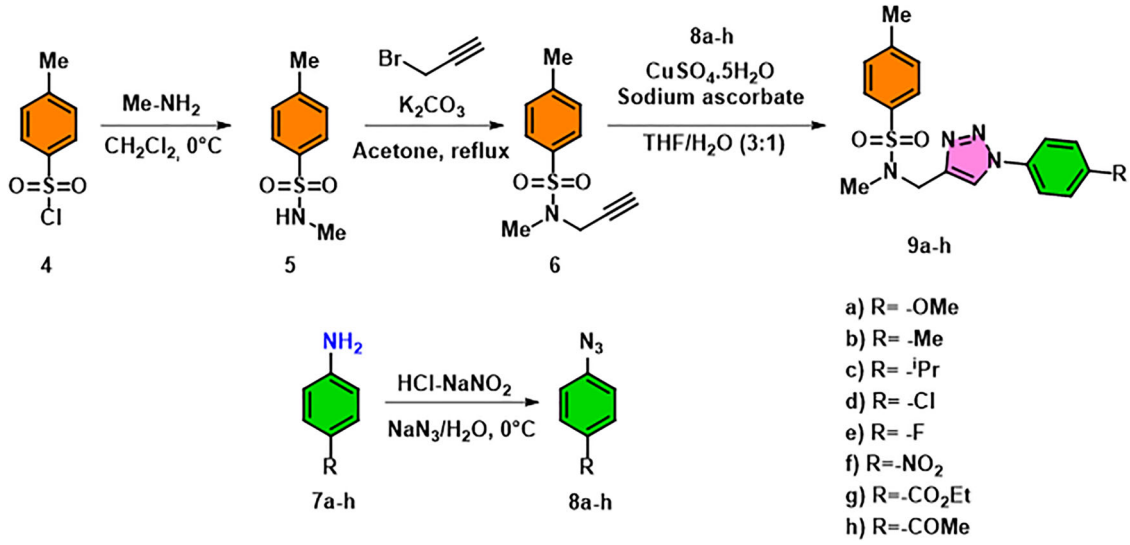

Figure 2. Schematic representation of the synthesis steps of **9a–h** compounds.

122.51, 122.43, 121.32, 116.90, 116.67, 45.61, 35.11, 21.53. Anal. calcd for $C_{17}H_{17}FN_4O_2S$ (%): C, 56.65; H, 4.75; N, 15.55; S, 8.90; Found (%): C: 56.67; H: 4.74; N: 15.53; S, 8.93.

N,4-dimethyl-N-((1-(4-nitrophenyl)-1H-1,2,3-triazol-4-yl)methyl)benzenesulfonamide (**9f**): Yield: 73%, m.p.: 170–172 °C, colour: Yellow, FTIR: 3122, 3096, 2911, 2815 (C-H), 1594, (C = C), 1514 (N-O), 1454 (N = N), 1334 (S = O). ^{1}H NMR (400 MHz, $CDCl_3$) δ 8.45 (dd, J = 9.1, 1.1 Hz, 2H), 8.19 (s, 1H), 8.00 (dd, J = 9.1, 1.1 Hz, 2H), 7.75 (d, J = 7.3 Hz, 2H), 7.39 (d, J = 8.3 Hz, 2H), 4.46 (s, 2H), 2.84 (s, 3H), 2.48 (s, 3H). ^{13}C NMR (100 MHz, $CDCl_3$) δ 147.35, 145.49, 143.96, 141.03, 134.43, 129.92, 127.45, 125.56, 121.19, 120.51, 45.56, 35.26, 21.54. Anal. calcd for $C_{17}H_{17}N_5O_4S$ (%): C, 52.71; H, 4.42; N, 18.08; S, 8.28; Found (%): C: 52.73; H, 4.40; N, 18.11; S, 8.25.

Ethyl-4-(((N,4-dimethylbenzenesulfonamido)methyl)-1H-1,2,3-triazol-1-yl)benzoate (**9g**): Yield: 83%, m.p.: 138–140 °C, colour: Light yellow, FTIR: 3124, 3096, 2987, 2915 (C-H), 1711 (C = O), 1598, 1518 (C = C), 1444 (N = N), 1366 (C-N), 1328 (S = O), 1274 (C-O). ^{1}H NMR (400 MHz, $CDCl_3$) δ 8.24 (d, J = 8.7 Hz, 2H), 8.08 (s, 1H), 7.85 (d, J = 8.8 Hz, 2H), 7.75 (d, J = 8.1 Hz, 2H), 7.38 (d, J = 8.1 Hz, 2H), 4.49 – 4.41 (m, 4H), 2.83 (s, 3H), 2.48 (s, 3H), 1.46 (t, J = 7.1 Hz, 3H). ^{13}C NMR (100 MHz, $CDCl_3$) δ 165.38, 144.79, 143.84, 139.86, 134.54, 131.34, 130.80, 129.88, 127.47, 121.02, 119.84, 61.48, 45.59, 35.16, 21.54, 14.31. Anal. calcd for $C_{20}H_{22}N_4O_4S$ (%): C, 57.96; H, 5.35; N, 13.52; S, 7.73; Found (%): C: 57.94; H, 5.36; N, 13.50; S, 7.74.

N-((1-(4-acetylphenyl)-1H-1,2,3-triazol-4-yl)methyl)-N,4-dimethylbenzenesulfonamide (**9h**): Yield: 57%, m.p.: 159–160 °C, colour: Yellow, FTIR: 3124, 2923 (C-H), 1675 (C = O), 1602, 1518 (C = C), 1442, 1412 (N = N), 1344 (C-N), 1326 (S = O), 1266 (C-CO-C). ^{1}H NMR (400 MHz, $CDCl_3$) δ 8.14 (d, J = 8.7 Hz, 2H), 8.10 (s, 1H), 7.87 (d, J = 8.7 Hz, 2H), 7.74 (d, J = 8.2 Hz, 2H), 7.37 (d, J = 8.1 Hz, 2H), 4.45 (s, 2H), 2.83 (s, 3H), 2.68 (s, 3H), 2.46 (s, 3H). ^{13}C NMR (100 MHz, $CDCl_3$) δ 196.52, 144.88, 143.85, 139.92, 137.01, 134.51, 130.12, 129.88, 127.46, 121.03, 120.03, 45.58, 35.17, 26.67, 21.53. Anal. calcd for $C_{19}H_{20}N_4O_3S$ (%): C, 59.36; H, 5.24; N, 14.57; S, 8.34; Found (%): C: 59.38; H, 5.23; N, 14.55; S, 8.32.

2.5. X-ray structures solution and refinement for the compounds

The method for single crystal X-ray crystallographic data for compounds **9a–e** is given in the supplementary section. Table 1 provides the crystal data and refining information.

2.6. Biological assays

Methods of all biological activity (ABTS, DPPH, Cuprac, AChE, BuChE and anticancer) studies of compounds (**9a–h**) are given in the supplementary section.

2.7. In silico ADMET and molecular docking studies

The method of *in silico* studies is shown in detail in the supplementary section.

3. Results and discussion

3.1. Chemistry

The synthesis of hybrid structures containing targeted 1,2,3 triazole and N-methyl-toluenesulfonamide groups was carried out by means of "click chemistry". For this purpose, firstly, aryl azides (8a–h) were synthesized. Then, N,4-Dimethyl-N-2-propyn-1-ylbenzenesulfonamide (6) compound was synthesized with the help of N,4-dimethylbenzenesulfonamide (5) and propargyl bromide. Hybrid structures were synthesized in high yields from the Cu(I) catalyzed reaction of N,4-Dimethyl-N-2-propyn-1-ylbenzenesulfonamide and aryl azides. Structural characterization of the synthesized compounds was elucidated using FT-IR, X-ray, ^{1}H(^{13}C)-NMR and elemental analysis techniques (Figure 1).

Table 1. Single crystal X-ray data and refinement details for compounds **9a–e**.

Identification code	9a	9b	9c	9d	9e
Empirical formula	$C_{18}N_4O_3SH_{20}$	$C_{18}H_{20}N_4O_2S$	$C_{20}H_{24}N_4O_2S$	$C_{17}H_{17}N_4O_2ClS$	$C_{34}H_{34}F_2N_8O_4S_2$
Formula weight	372.44	356.44	384.49	376.85	720.81
Temperature/K	293(2)	293(2)	293(2)	293(2)	293(2)
Crystal system	Monoclinic	Monoclinic	Orthorhombic	Triclinic	Triclinic
Space group	$P2_1/c$	$P2_1/c$	$Pna2_1$	P-1	P-1
a/Å	13.1702(5)	5.5339(3)	33.671(2)	5.6539(6)	5.6384(4)
b/Å	5.6300(2)	35.8595(19)	10.4648(8)	10.2494(14)	9.8797(7)
c/Å	24.5402(9)	9.0757(6)	5.6865(3)	16.1089(16)	16.2802(12)
α/°	90	90	90	92.660(10)	78.923(6)
β/°	96.915(4)	96.501(7)	90	97.125(9)	81.556(6)
γ/°	90	90	90	105.376(11)	74.329(6)
Volume/Å^3	1806.38(12)	1789.43(18)	2003.7(2)	890.06(18)	852.58(11)
Z	4	4	4	2	1
ρ_{calc} g/cm^3	1.369	1.323	1.275	1.406	1.404
μ/mm^{-1}	0.205	0.200	0.184	0.350	0.219
2Θ range for data collection/°	6.71 to 55.306	7.26 to 55.712	7.196 to 55.576	6.84 to 58.004	7.228 to 57.508
Reflections collected	5675	6023	5675	6779	6434
Independent reflections	3555 [R_{int} = 0.0157, R_{sigma} = 0.0361]	3532 [R_{int} = 0.0234, R_{sigma} = 0.0499]	3014 [R_{int} = 0.0218, R_{sigma} = 0.0351]	4044 [R_{int} = 0.0386, R_{sigma} = 0.0856]	3847 [R_{int} = 0.0244, R_{sigma} = 0.0452]
Data/restraints/parameters	3555/0/239	3532/0/230	3014/1/249	4044/0/229	3847/0/228
Goodness-of-fit on F^2	1.022	1.061	1.064	0.960	1.051
Final R indexes [I> =2σ (I)]	R_1 = 0.0420, wR_2 = 0.0960	R_1 = 0.0580, wR_2 = 0.1171	R_1 = 0.0447, wR_2 = 0.0918	R_1 = 0.0548, wR_2 = 0.1043	R_1 = 0.0519, wR_2 = 0.1172
Final R indexes [all data]	R_1 = 0.0586, wR_2 = 0.1052	R_1 = 0.0936, wR_2 = 0.1367	R_1 = 0.0567, wR_2 = 0.1000	R_1 = 0.1166, wR_2 = 0.1350	R_1 = 0.0822, wR_2 = 0.1386
Largest diff. peak/hole / e Å^{-3}	0.22/-0.26	0.24/-0.23	0.23/-0.17	0.24/-0.38	0.23/-0.27
CCDC	2095525	2095527	2095526	2095528	2095529

3.2. Spectroscopic characterization of the 9a-h compounds

Common analytical methods (FT-IR, X-ray, $^{1}H(^{13}C)$-NMR and elemental analysis) were used in the characterization of these new hybrid structures and spectroscopic data were given in the experimental section. The presence of characteristic bands in the FTIR spectra of hybrid forms confirms the structures.

Characteristic signals of aryl azide and alkyne units observed around 2132–2091 cm^{-1} in FTIR spectra disappeared. This indicates that the relevant functional groups have reacted. In addition, new signal pairs, which should be present in triazole hybrid structures and reveal the presence of $-SO_2-$ groups, are seen at approximately 1400–1300 and 1200–1000 cm^{-1}. The characteristic carbonyl band, which should be present in 9g and 9h structures, is also seen at 1711 and 1675 cm^{-1} (Figures S1–S18).

The $^{1}H(^{13}C)$-NMR data of the hybrid structures are given in the experimental section, and their spectra are given in the auxiliary materials (Figures S19–S38). NMR spectra of all structures will not be discussed individually but will be explained with the help of $^{1}H(^{13}C)$-NMR spectra of compound **9a** as a model. It belongs to a proton in the singlet triazole ring observed at 9.91 ppm in the spectrum (Figure S23). The protons of the phenyl rings in the hybrid structure resonated, giving two separate AB systems. AB system given by aryl protons belonging to the tosyl group is seen at 7.74 (d, $J = 7.9$ Hz) and 7.37 (d, $J = 7.8$ Hz) ppm. The AB system of the protons of the phenyl ring attached to the triazole is seen at 7.62 (d, $J = 8.6$ Hz, 2H) and 7.04 ppm (d, $J = 8.6$ Hz, 2H). Methylene protons adjacent to the nitrogen in the structure gave singlet at 4.42 ppm, and methoxy protons at 3.89 ppm. The singlets seen at 2.81 and 2.47 ppm belong to the methyl groups attached to the nitrogen atom and in the tosyl group.

In the ^{13}C-NMR spectrum of triazole **9a** (Figure S24), aromatic carbon signals appear in the range of 159.95–114.82 ppm. In the spectrum, the resonance signal of methoxy carbon is seen at 55.64 ppm, the signals of methylene and methyl carbons adjacent to nitrogen are seen at 45.63 and 35.04 ppm. The methyl carbon in the tosyl group is seen at 21.52 ppm. The ^{1}H and ^{13}C-NMR spectra of the structures are in full agreement with the structures.

3.3. Crystal structures of 9a–9e

Crystal structures of compounds **9a–e** are given Figure 3. The structures of all compounds are similar differing principally in the substitute group on the phenyl ring (C12–C17). In all compounds, the bond distances and angles in the sulfonamide unit are within the range of expected values. The S atom in the compounds show a distorted tetrahedral geometry and the S-O bond distances are within the range of 1.426–1.433 Å, comparable to those reported structures (Perlovich et al., 2013). In the structures, 1,2,3-triazole rings show the aromatic character with expected bond lengths and angles (Cunha et al., 2016). In the structures of all compounds (**9a–e**), molecules are linked by C-H·····N interactions forming supramolecular chains. Packing diagram of compound **9a** showing C-H·····N contacts is given in Figure 4. The crystal structures of the compounds are further stabilized by C-H·····O and C-H·····π contacts.

3.4. Antioxidant activity

Antioxidant properties, especially radical scavenging activities, are very important due to the removal of harmful effects of free radicals in biological systems. $DPPH^{\bullet}$ and $ABTS^{\bullet+}$ have been widely used to analyze the free radical scavenging efficacy of various antioxidant substances. In this study, the antioxidant activity of the newly synthesized compounds **9a–h** and standard antioxidants such as, BHT, α-Tacoferol and Ascorbic acid were determined using $DPPH^{\bullet}$ and $ABTS^{\bullet+}$ methods. The samples were examined for their radical scavenging capabilities ranging between 12.50 and 100 μg/mL concentrations. Table 2 defines a significant decrease ($p < 0.05$) in the concentration of $DPPH^{\bullet}$ radical due to the scavenging ability of compounds and standards.

The scavenging effect of compounds **9a–h** and standards on the $DPPH^{\bullet}$ radical decreased in the order of **Ascorbic acid** > **α-Tacoferol** > **9f**> **9h** > **BHT** > **9d** > **9b** > > **9g** > **9a** > **9c** > **9e**, which were 78.70, 24.63, 44.08, 21.79, 19.66, 17.48, 17.40, 15.82, 14.78, 13.61, 13.55, 11.90% at the concentration of 100 μg/mL, respectively. Free radical scavenging activity of these samples also increased with an increasing concentration. $DPPH^{\bullet}$ radical scavenging activity is shown in Figure 5.

IC_{50} values of $DPPH^{\bullet}$ radical scavenging was found as 367.37 μg/mL for **9a**, 316.05 μg/mL for **9b**, 369.01 μg/mL for **9c**, 287.35 μg/mL for **9d**, 420.16 μg/mL for **9e**, 229.46 μg/mL for **9f**, 338.29 μg/mL for **9g**, 254.32 μg/mL for **9h**, 203.21 μg/mL for α-Tacoferol, 63.53 μg/mL for Ascorbic acid, 286.04 μg/mL for **BHT**. The $DPPH^{\bullet}$ scavenging effect of all compounds and standards decreased in the following order: of **Ascorbic acid** > **α-Tacoferol** > **9f**> **9h** > **BHT** > **9d** > **9b** > **9g** > **9a** > **9c** > **9e**. A lower IC_{50} value indicates a higher $DPPH^{\bullet}$ free radical scavenging effect (Table 2). The DPPH activity of 9f and 9h are higher than BHT, while the lowest activities belong to **9d, 9b, 9g, 9a, 9c** and **9e.**

All tested compounds exhibited effective radical scavenging activity against $ABTS^{\bullet+}$ radicals ($p > 0.001$). As seen in Figure 4, all compounds had effective $ABTS^{\bullet+}$ radical scavenging activity in a concentration dependent manner (12.5–100 μg/mL). The scavenging effect of compounds and standards on the $ABTS^{\bullet+}$ radicals decreased in the order of **Ascorbic acid** > α-Tacoferol > **BHT** > **9c** > **9e** > **9b** > **9h** > **9d** > **9f** > **9g** > **9a**, which were 93.10, 72.30, 66.43, 66.26, 65.41, 64.67, 64.10, 63.41, 63.47, 62.84, 62.27% at the concentration of 100 μg/mL, respectively. Free radical scavenging activity of these samples also increased with an increasing concentration.

IC_{50} values for compounds **9a–h** were calculated as 10.25 μg/mL for **9a**, 15.36 μg/mL for **9b**, 10.45 μg/mL for **9c**, 10.02 μg/mL for **9d**, 10.05 μg/mL for **9e**, 10.20 μg/mL for **9f**, 10.22 μg/mL for **9 g**, 10.19 μg/mL for **9h**. On the other hand,

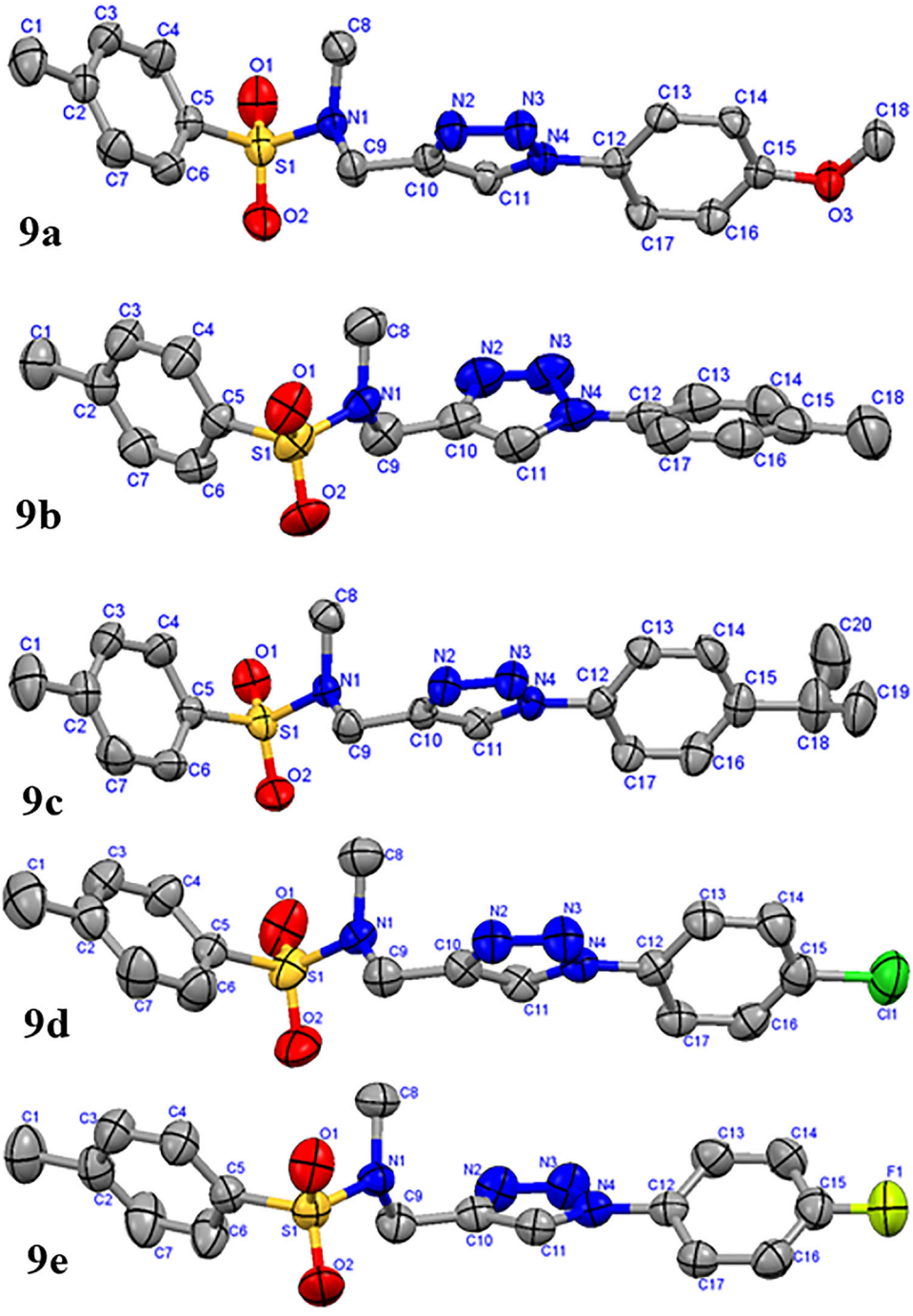

Figure 3. Thermal ellipsoid (50% probability) plots for **9a–e** with atom numbering.

IC_{50} values were found as for 8.74 μg/mL for ascorbic acid, 9.58 μg/mL for **BHT** and, 11.25 μg/mL for **α-Tacoferol** (Table 2). The $ABTS^{\bullet+}$ scavenging effect of all compounds and standards decreased in the following order of Ascorbic acid > **α-Tacoferol > BHT > 9c > 9e > 9b >9h > 9d > 9f > 9g > 9a**. As with the $DPPH^{\bullet}$ method, a lower IC_{50} value indicates a higher $ABTS^{\bullet+}$ radical scavenging ability. All compounds showed similar $ABTS^{\bullet+}$ radical scavenging ability to standarts.

The values of the CUPRAC method, in which the chromogenic neocuproine was used as the oxidizing agent, are shown in Table 2. All synthesized compounds showed less activity than α-Tocopherol, and ascorbic acid. The **9d**, **9f**, **9g**, and **9h** are active compounds. At the same concentration (100 μg/mL), reducing capacities decreased in the order of **Ascorbic acid > α-Tocopherol >9f ≥ 9g > 9h > 9c > BHT ≥ 9b ≥ 9e > 9a > 9d.**

3.5. Cholinesterase enzymes inhibition assay

Cholinesterase inhibitors (ChE) are among the most important therapeutic agents in the treatment of Alzheimer's disease (AD). Cognitive function was found to be stable for approximately one year in approximately 50% of the patients examined (Giacobini, 2001, 2004). Studies have shown that both acetylcholinesterase (AChE) and butyrylcholinesterase

(BuChE) play a role in breaking down acetylcholine in the brain. It is known in the literature that dual inhibition of these enzymes will increase the efficacy of treatment of the disease (Anand & Singh, 2013; Raina et al., 2008). All synthesized compounds were investigated for their properties as AChE and BuChE inhibitors. The inhibitory potency of the synthesized compounds was defined as half the maximum inhibitory concentration, IC50. Enzymes (electric eel acetylcholinesterase (AChE) and horse serum butyrylcholinesterase (BuChE) were commercially procured and inhibition studies of all compounds were performed in-vitro using the spectrophotometric method. Galantamine was used as the standard drug. The results are summarized in Table 3. It is evident that most of the synthesized compounds exhibit good to moderate inhibitory activities. IC_{50} values for AChE range from 13.81 to 38.98 μM and for BuChE from 172.46 to 52.48 μM. All synthesized compounds were found to be significantly active against AChE from BuChE. Experimental results showed that these compounds are relatively more inhibitors of AChE compared to BuChE. This result is attributed to the relatively smaller active site of the AChE enzyme, which is able to assimilate the smaller one. In contrast to the broader active region of the BuChE enzyme, although all the structural features were actively involved in the inhibitory activity, the variation of different groups on the main structural motif was actually responsible for the change in inhibitory potential. Compound (**9c**) containing isopropyl at the 4′ position of the phenyl ring is the most active AChE (IC_{50}=13.81 μM) among the series. The compound with the second best AChE (IC_{50} = 15.13 μM) inhibitory property is the compound (9a) containing the -OMe group. Effects of –OMe groups the hydrophobic character of the flexible group and the presence of –O atoms as potential proton acceptors in hydrogen bond formation may provide access to the enzyme binding site. Mainly, this alkyl group is thought to result from hydrophobic interactions with the nonpolar pockets of the predicted enzymes. The next most potent dual inhibitor is compound (**9h**) containing a methyl ketone group at the 4′ position of the phenyl ring (IC_{50}= 15.53 μM for AChE and 56.45 μM for BuChE). Similar to Galantamine, it has a small selectivity for AChE over BuChE (Orhan et al., 2019). Interestingly, compounds (**9c**) and (**9a**) are much weaker inhibitors to BuChE compared to AChE, indicating that these compounds can serve as selective inhibitory agents for AChE.

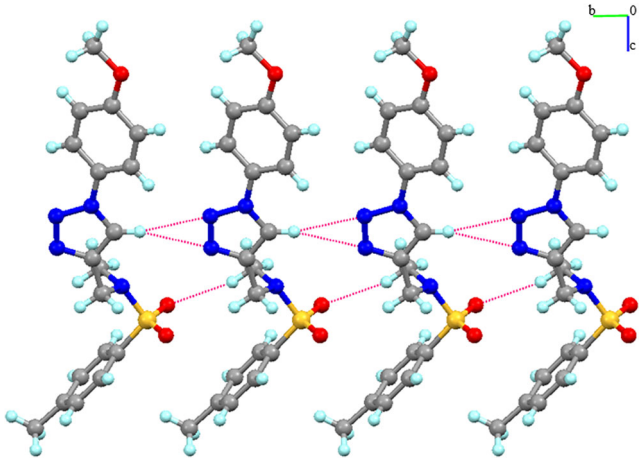

Figure 4. The C-H·····N interactions along the axis in the structure of **9a**.

3.6. Enzyme kinetics

The IC_{50} values of 8 compounds and Galantamine selected in the enzyme activity assay against AChE and BuChE are given in Table 3. The selectivity index (SI) was calculated to determine whether the compounds were selective for enzymes. It can be determined that compounds with a selectivity index greater than one may be more selective for that enzyme. It is known that compounds with a lower IC_{50} value greater than one is more selective against AChE, but those close to one exhibit dual inhibition. The results clearly show that 8 synthesized compounds are AChE inhibitors. As compounds **9a** and **9c** showed almost 10 times higher enzyme inhibition than Galantamine, enzyme kinetic studies of these compounds were performed.

Acetylthiocholine iodide was used as substrate for AChE inhibition. The Lineweaver-Burk plot of 1/V versus substrate 1/[S] in the presence of different inhibitor concentrations (5, 10 and 20 μM) resulted in a series of solid lines for AChE as shown in Figure 5. The type of inhibition of compounds, ie whether they are competitive or not, can be determined by the Lineweaver-Burk plot. Inhibition-type competitive graphs

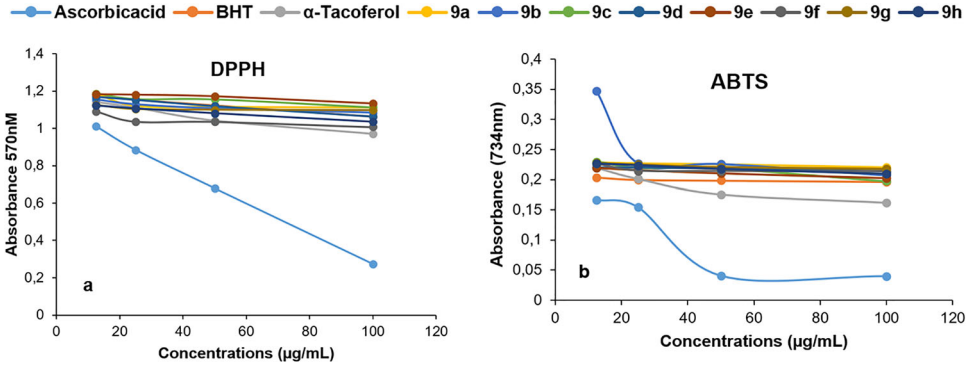

Figure 5. DPPH and ABTS free radical scavenging activity of different concentrations (12.5–100 μg/mL) of compound **9a–h** and reference antioxidants; BHT, α-Tacoferol and Ascorbic acid (BHT: butylated hydroxytoluene; DPPH: 1,1-diphenyl-2-picryl-hydrazyl free radical).

Table 2. Determination of half maximal concentrations (IC_{50}, μg/mL) of compounds **9a–h** and standards for $DPPH^{\bullet}$, $ABTS^{\bullet+}$ scavenging and (Cu^{2+}) reducing capacity.

Compounds	$DPPH^{\bullet}$ scavenging IC_{50}	$ABTS^{\bullet+}$ scavenging IC_{50}	Cu^{2+}- Cu^{+} reducing λ_{450}*
Ascorbic acid	63.53 ± 0.001	8.74 ± 0.002	0.299 ± 0.002
BHT	286.04 ± 0.003	9.58 ± 0.003	0.066 ± 0.001
α-Tacoferol	203.21 ± 0.002	11.25 ± 0.003	0.102 ± 0.001
9a	367.37 ± 0.001	10.25 ± 0.001	0.065 ± 0.001
9b	316.05 ± 0.004	15.36 ± 0.003	0.066 ± 0.005
9c	369.01 ± 0.005	10.45 ± 0.001	0.071 ± 0.003
9d	287.35 ± 0.001	10.02 ± 0.004	0.063 ± 0.001
9e	420.16 ± 0.006	10.05 ± 0.005	0.066 ± 0.001
9f	229.46 ± 0.001	10.20 ± 0.002	0.087 ± 0.013
9g	338.29 ± 0.001	10.22 ± 0.003	0.087 ± 0.005
9h	254.32 ± 0.002	10.19 ± 0.001	0.083 ± 0.001

Table 3. AChE and BuChE enzyme inhibition results of **9a–h** compounds and standard Galantamine.

	IC_{50} (μM)		Selectivity (SI)
Compounds	EeAChE	eqBuChE	EeAChE/eqBuChE
9a	15.13 ± 0.050	109.26 ± 0.40	7.22
9b	38.98 ± 0.035	163.93 ± 0.07	4.20
9c	13.81 ± 0.0026	122.81 ± 6.13	8.89
9d	26.56 ± 0.032	172.46 ± 1.86	6.49
9e	33.93 ± 0.035	156.59 ± 2.05	4.61
9f	21.14 ± 0.047	92.66 ± 0.42	4.38
9g	26.79 ± 0.0053	52.48 ± 0.27	1.96
9h	15.53 ± 0.0045	56.45 ± 1.0	3.63
Galantamine	136 ± 0.008	82 ± 0.15	1.65

have non-diagonal parallel lines (Makarian et al., 2022). If the x and y axes do not intersect at the same point as the lines, it is called a mixture type. If they intersect at the same point on the *y*-axis but have different slopes and intersections, they are reported as competitive. Non-competitive have the same intersection on the *x*-axis but different slopes and intersections on the *y*-axis. According to the above-mentioned studies, a competitive inhibition was attributed to AChE for **9a** compound, while a mixed type of inhibition was found for the **9c** compound. The slopes and intersections increase with increasing concentration of inhibitor. A secondary plot of the slope versus inhibitor concentration was plotted and the inhibition constant (Ki) found to be 0.23 and 0.26 μM was calculated (Figure 6).

3.7. Anticancer activity results

The cytotoxicity of compounds **9a**–**h** was evaluated against A549 (non-small cell lung carcinoma) cell lines by CVDK. Anticancer activities of synthesized compounds **9a–h** were compared with *cis*-platin using the CVDK assay. *Cis*-platin, one of the most used anticancer drug in cancer, was used as a positive control (IC_{50} value for A549 cell line: 6.202 μM) (Reedijk, 1996). According to the IC_{50} values of the newly synthesized compounds, compounds **9d** (IC_{50} = 3.81 μM) and **9g** (IC_{50}= 4.317 μM) showed quite strong activity against the A549 cell line compared to *cis*-platin. Of the compounds, **9c** (IC_{50}=7.087 μM) and **9h** (IC_{50}= 6.979 μM) showed anticancer activity close to *cis*-platin. These molecules with the strongest activity values have, respectively, Cl, ester, isopropyl and ketone groups at the 4′ position of the phenyl ring. It can be said that substituents other than isopropyl have strong activity values due to their bulky groups, polar-apolar centers and H bonds. On the other hand, the isopropyl group is thought to show activity as it can make hydrophobic interactions with apolar pockets of biotargets. Although other compounds showed weaker activity than *cis*-platin, they showed activity in the micromolar activity against the A549 cell line (Table 4).

On the other hand, the cytotoxic effect of compounds **9a–h** on non-cancerous human dermal fibroblast cell (HDF) was also assessed. According to the results, compound **9d** (IC_{50} on A549: 3.81 μM) was up to twice more potent than *cis*-platin against the A549 cell line while close toxic than cisplatin (IC_{50} on HDF: 61.76 μM) against HDF cell line. On the other hand, not only the anticancer activity of compounds **9c** and **9h** was close to that of cisplatin on the A549 cell line, but also these compounds were a little more toxic than cisplatin against the HDF cell line. Furthermore, **9f** was the most toxic between all tested compounds (Table 4).

3.8. In silico ADMET prediction

A lot of time, effort, and budget is needed for the lengthy and challenging process of discovering and developing new drugs. Because they are usually found to be useless or pose serious health risks and have negative impacts, drug candidates have a high dropout rate. Estimates suggest that up to 40% of drug candidates have failed due to toxicity in the past, accounting for almost half of all failures in terms of efficacy (Wan, 2013). Because of this, drug development must pay close attention to ADME/Tox (Absorption, Distribution, Metabolism, Elimination, Toxicity). These investigations cover crucial issues for every aspect of ADMET, enabling the viability of drug candidates to be determined. In the early stages of drug candidate molecules, ADMET data makes it easier to choose and calculate the therapeutic dose of substances with the best safety profiles, which expedites the drug discovery process. As a result, the growing drug design process' evaluation times are cut short, saving time and vital resources. (Isika et al., 2022).

Several properties of drug-like qualities can be quantified through physicochemical metrics, which may be determined *in silico*. Libraries can be filtered using criteria like the "Lipinski Rule of Five" to weed out molecules with poor potential drug-like characteristics that merely serve to waste costly drug development resources. The Lipinski rule (molecular weight <500, not more than five hydrogen bond donors, not more than ten hydrogen bond acceptors and a partition coefficient (log P) value <5) states that an orally

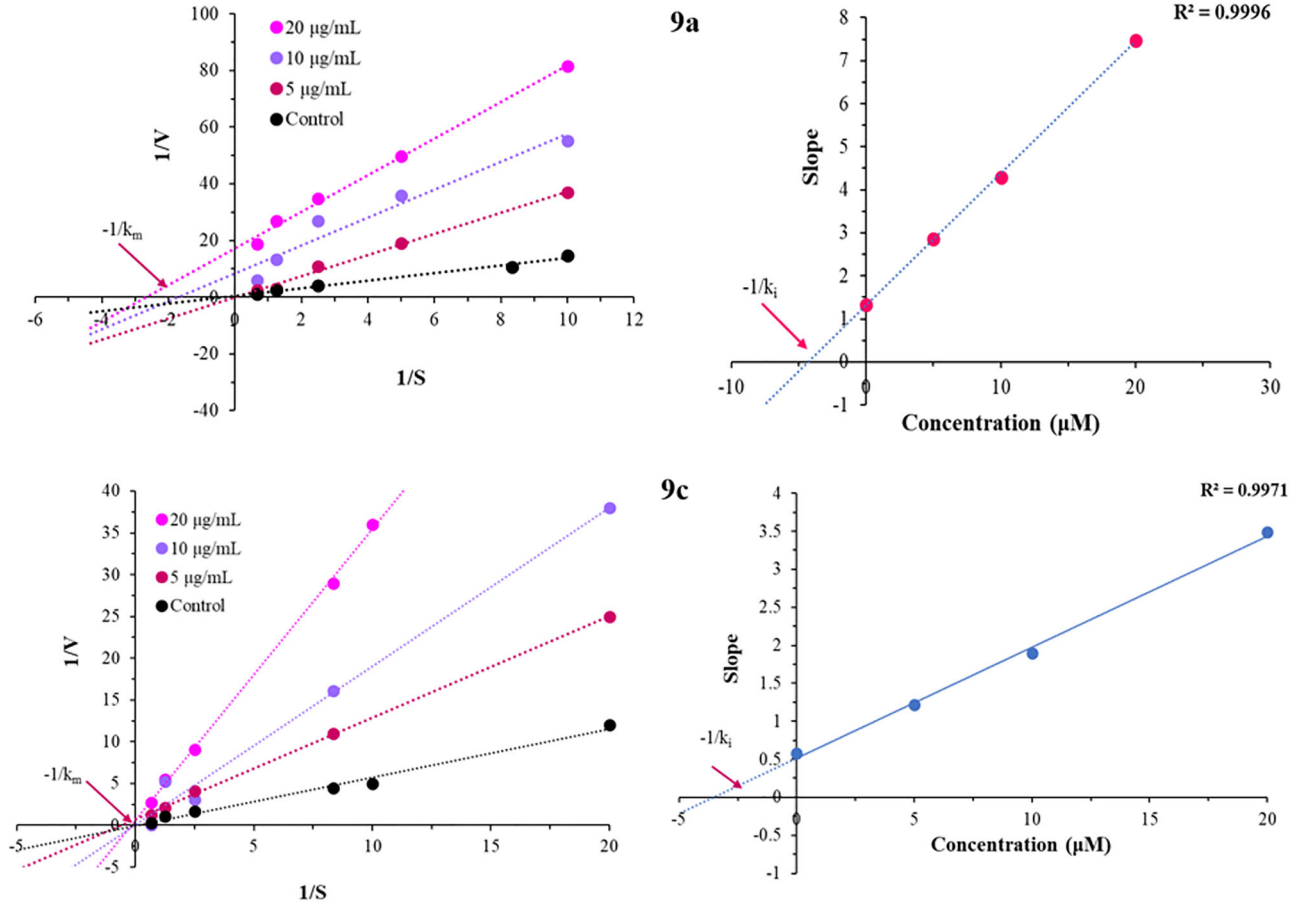

Figure 6. Kinetic study of AChE inhibition by compound **9a** and **9c**. The Lineweaver-Burk reciprocal plot of AChE initial velocity with increasing substrate concentrations is illustrated in panel. The slopes of the lines for 1/V vs. 1/[S] from the LWB plot were plotted against the concentration of inhibitor to construct the secondary plot shown in panel (b). V = initial velocity rate, [S] = concentration of substrate, [I] = concentration of inhibitor **9a** and **9c**.

Table 4. IC_{50} values of compounds **9a–h** on A549 and HDF cell lines.

	IC_{50}(µM)	
Compounds	A549	HDF
9a	21.39 ± 0.0695	60.16 ± 0.0441
9b	25.95 ± 0.0454	52.48 ± 0.0159
9c	7.087 ± 0.0153	51.59 ± 0.0607
9d	3.81 ± 0.1084	45.84 ± 0.0664
9e	42.54 ± 0.1541	173.6 ± 0.0331
9f	65.6 ± 0.0337	39.75 ± 0.0505
9g	4.317 ± 0.0367	50.89 ± 0.0229
9h	6.979 ± 0.0613	48.59 ± 0.0325
cis-platin	6.202 ± 0.0705	61.76 ± 0.0478

Cells were treated with concentrations ranging from 6.25 to 200 µM for 48 h.

bioactive drug or therapeutic candidate should not have more than one violation (Lipinski, 2004). The swissADME online software application was used to conduct *in silico* ADME screening on synthetic compounds to forecast drug scores overall and physicochemical characteristics (Şahin et al., 2022b). According to Lipinski's rule of five, the ADME data gathered from the calculations showed that all synthetic compound values remained within the established boundaries. The synthesized compounds adhered strictly to and did not break any Lipinski rules, according to all the requirements mentioned in Table 5. The percentage of absorption of the molecules was calculated using the table's data (using the formula: %ABS = 109 − 0. 345 × TPSA) and ranged from 66.81 to 82.67.

Lipophilicity is the ability of a lipid media to disperse in water. Drug molecules must pass through various biological membranes, including the blood–brain barrier (BBB), the skin, and the gut, to reach their target areas. Therefore, a compound must be dissolved in water and lipid at certain rates. The lipophilicity values of the compounds XLOGP3 (Log Po/w) are in the range of 2.07 and 3.52. The solubility of compounds is high, and the value is between −3.41 and −4.21.

The enzymes in the superfamily known as cytochrome P450 (CYP) inhibitors, typically called liver enzymes and isoenzymes, play a role in the metabolism of numerous drugs by catalyzing different oxidation processes (Kar & Leszczynski, 2020). The five most crucial human versions are CYP2D6, CYP2C9, CYP3A4, CYP1A2 and CYP2C19, and at least one of the CYP enzymes is involved in the metabolism of more than 90% of all therapeutics available today. Therefore, it is crucial to establish whether a chemical is a cytochrome P450 substrate. Although substances can often activate or inhibit several of these enzymes, it was assumed that they did not simply interact with the CYP2D6 inhibitor.

For a quick evaluation of drug similarity, SwissADME-specific bioavailability radar plots of drugs were analyzed. The six physicochemical parameters revealed in this radar plot are lipophilicity (LIPO), size (SIZE), polarity (POLAR), solubility (INSOLU), flexibility (FLEX), and saturation (INSATU). An oral bioactive drug's affinity characteristics are graphically assessed

Table 5. Physicochemical, pharmacokinetics and drug-likeliness properties of synthetic compounds according to the rule of five.

		Compound							
Properties	Rule	9a	9b	9c	9d	9e	9f	9g	9h
MW	<500	372.44	356.44	384.5	376.86	360.41	387.41	414.48	384.45
#Rotatable bonds	≤ 9	6	5	6	5	5	6	8	6
#H-bond acceptors	≤ 10	6	5	5	5	6	7	7	6
#H-bond donors	≤ 5	0	0	0	0	0	0	0	0
MR		98.1	96.57	106.19	96.62	91.57	100.43	107.7	101.8
TPSA (Å^2)	<130	85.7	76.47	76.47	76.47	76.47	122.29	102.77	93.54
XLOGP	≤ 5	2.36	2.75	3.52	3.02	2.49	2.22	2.61	2.07
ESOL Log S		−3.72	−3.96	−4.51	−4.25	−3.82	−3.71	−3.96	−3.6
% Absorption		79.44	82.62	82.62	82.62	82.62	66.81	73.55	76.73
GI absorption		High	High	High	High	High	High	High	High
BBB permeant		No	Yes	No	Yes	Yes	No	No	No
Pgp substrate		No	No	No	No	No	No	No	No
CYP1A2 inhibitor		No	Yes	No	Yes	Yes	No	No	No
CYP2C19 inhibitor		Yes	Yes	Yes	Yes	Yes	Yes	Yes	Yes
CYP2C9 inhibitor		Yes	Yes	Yes	Yes	Yes	Yes	Yes	Yes
CYP2D6 inhibitor		No	No	No	No	No	No	No	No
CYP3A4 inhibitor		Yes	Yes	Yes	Yes	No	Yes	Yes	Yes
log Kp (cm/s)		−6.9	−6.52	−6.15	−6.45	−6.73	−7.09	−6.98	−7.18
Lipinski violations (LV)	≤ 1	0	0	0	0	0	0	0	0
Bioavailability Score		0.55	0.55	0.55	0.55	0.55	0.55	0.55	0.55
PAINS #alerts		0	0	0	0	0	0	0	0
Brenk #alerts		0	0	0	0	0	2	0	0
Synthetic Accessibility		3.07	3.08	3.26	3	2.97	3.11	3.3	3.08

Key: MW: Molecular weight (gr/mol), %Abs: Percentage of absorption, TPSA: Topological polar surface area, RB: number of rotatable bonds, HBA: number of hydrogen bond acceptors, HBD: number of hydrogen bond donors, LV: number of Lipinski rule of 5 violations, Log Po/w (iLOGP): Lipophilicity, BS: Bioavailability score, SA: Synthetic accessibility [From 1 (very easy) to 10 (very difficult)], WS: Water solubility Log S (Insoluble < −10 < Poorly < −6 < Moderately < −4 < Soluble < −2 Very < 0 < Highly) Lipinski RO5: Molecular mass less than 500 Dalton, High lipophilicity (expressed as LogP less than 5), Less than 5 hydrogen bond donors, Less than 10 hydrogen bond acceptors; Molar refractivity should be between 40 and 130.

by this radar plot (Şahin et al., 2022b). The default SwissADME identifiers were used to produce the radar plot range, which is displayed as a pink region on each axis; the pink area in the radar plot defines the boundaries of these descriptors, and a chemical must fall within the radar plot to be considered drug-like (pink hexagon). If the TPSA score is higher than 130 Å^2, the compound's oral bioavailability is low (Daina et al., 2017). For all compounds, the TPSA value ranges from 76.47 to 122.29. All synthetic compounds have a high oral bioavailability profile, according to the bioavailability radar charts, which is consistent with this approach (Figure 7).

The entry of a drug candidate molecule into the lymphatic and blood circulation is influenced by a variety of characteristics, including the molecule's size, molecular weight, hydrophilic and lipophilic structure, and surface area and polarity. A boiled egg diagram of the compounds is shown in Figure 8. This diagram's focus is a simple technique to forecast two important ADME abilities at once: brain access and passive gastrointestinal absorption (HIA) (BBB). This categorization model was carefully created for statistical significance and resilience even though it only uses two physicochemical descriptors (WLOGP and TPSA for lipophilicity and apparent polarity, respectively) (Khalid et al., 2018). The gray, white, and yellow (yolk) zones on the boiled egg chart are separated by borders. No region is dependent on another. Compounds in the outer gray area have properties that indicate minimal absorption and limited BBB penetration. The blue dots in the diagram represent molecules that P-glycoprotein is predicted to excrete from the central nervous system, while the red dots represent molecules that are not predicted to be excreted. These dots in the white area indicate that the molecules are well absorbed in the gastrointestinal tract but cannot cross the BBB. If these dots are in the yellow area, this means that the compounds have a high rate of absorption through the gastrointestinal tract and a quick passage through the BBB (Daina & Zoete, 2016). When the boiled egg diagram of the synthetic compounds was analyzed, it was projected that three compounds (**9b**, **9d** and **9e**) could penetrate the BBB and that there was high absorption of all the molecules in the gastrointestinal tract. Accordingly, all molecules are positioned within the range within limits defined in drug candidates. A good manifestation of oral bioavailability can be expected when the parameters from ADME data are evaluated with the RO5 guidelines and the potential pharmacological effects of the compounds as prodrugs are based on the calculated absorption values.

The pkCSM web tool (http://biosig.unimelb.edu.au/pkcsm/) was used to predict the toxicity properties of the synthesized molecules (Pires et al., 2015). pkCSM is an online server database that can be used to calculate the toxicological properties of small molecules. This tool describes the toxicological effects of compounds such as AMES toxicity, human maximum tolerated dose, hERG-I inhibitor, hERG-II inhibitor, LD50, LOAEL, hepatotoxicity, skin toxicity, *T. pyriformis* toxicity, and Minnow toxicity. Table 6 presents information on the chemicals' predicted toxicity. According to the pkCSM web server results, none of the compounds except 9f were predicted to exhibit AMES toxicity. In addition, not all compounds inhibit hERG-I and hERG II and are not estimated to cause skin sensitization. The maximum tolerated dose, which should be ≤ 0.477 log (mg/kg/day) for compounds, has values ranging from −0.158 log (mg/kg/day) to 0.276 log (mg/kg/day). It has been anticipated that the compounds may

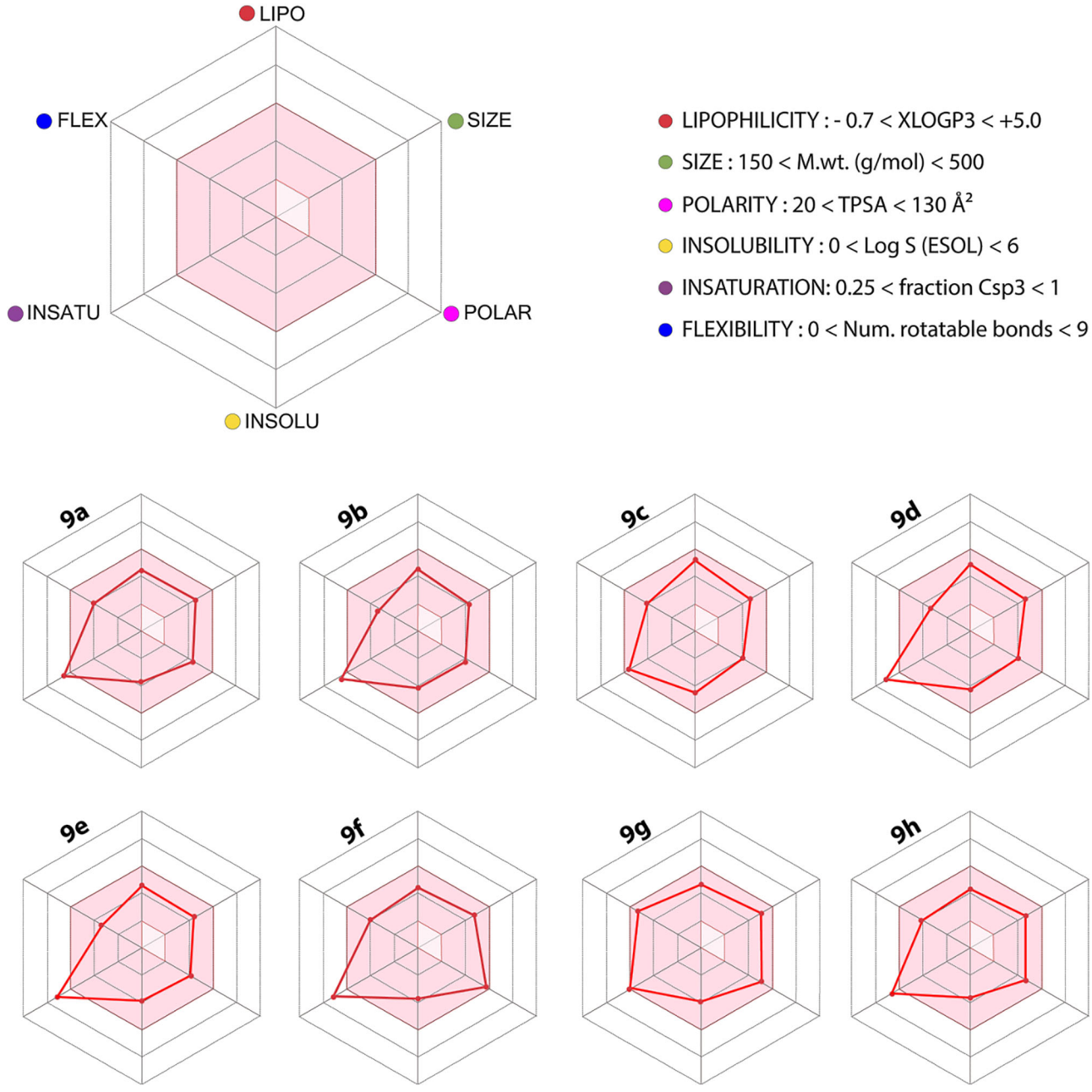

Figure 7. Bioavailability radar pertinent to physicochemical properties of compounds (**9a–h**).

exhibit hepatotoxicity if taken in excess of the maximum tolerated dose. Lethal dosage values (LD50) are a metric for acute toxicity commonly used to compare the toxicities of various compounds. The LD50 is the amount of compound administered at one time that causes the death of 50% of a group of test animals. These values are in the range of 2.112–2.919 mol/kg for compounds. In many therapeutic regimens, prolonged low- to moderate-dose chemical exposure is of substantial concern. Studies aim to determine the maximum dose at which no adverse effects are recorded and the lowest dose of a substance at which an observed adverse effect (LOAEL) occurs. The oral rat chronic toxicity [log(mg/kg bw/day)] values of the compounds were calculated in the range of 0.893 and 1.108. The results of the LOAEL must be evaluated considering the necessary bioactive concentrations and treatment times. *T. pyriformis* is a protozoa bacterium, and it is extensively employed as a toxic endpoint because of its toxicity. The plGC50 (negative logarithm of the concentration needed to block 50% growth in log μg/L) is expected for a specific substance and a value greater than −0.5 log μg/L is considered hazardous. All compounds showed *T. pyriformis* toxicity in the range of 0.391–0.667 log μg/L, with values well above the reference limit. Minnow toxicity values of the compounds were estimated from −0.453 to −1.374 ((log mM). A log LC50 is calculated for each substance in the Minnow toxicity database. LC50 values below 0.5 mM (log LC50 − 0.3) indicate significant acute toxicity.

3.9. Molecular docking studies

Molecular docking is a computational technique used in drug discovery and development to predict the binding

affinity of a small molecule to a target protein. The goal of molecular docking is to identify the best fit between the small molecule and the protein so that the small molecule can bind to the protein and potentially modulate its function (Çeşme, 2023; Isika et al., 2022; Yeşilkaynak et al., 2022).

Molecular docking analysis of synthetic compounds was performed to support and validate the results obtained from *in vitro* AChE inhibition experiments. To validate the molecular docking procedure, we compared the predicted binding poses of the ligand (Galantamine: GNT604) in the protein-ligand complex to the known crystal structure of the 4EY6 protein. This protein was used in our study as a reference. To perform the docking procedure, we selected the receptor grid for the AChE enzyme by restricting it to the residues occupied by the galantamine ligand and interacting with the ligand area. To do this, we removed the ligand (Galantamine) from the X-ray crystal structure of the AChE enzyme and re-docked it to the protein's binding site. Then, we compared the pose of the ligand in the enzyme's crystal structure to the pose obtained by re-docking and calculated the mean square deviation (RMSD) value. The results showed that the co-crystallized ligand had similar orientations and conformational poses as in the crystal structure when re-docked at the active binding sites of the target enzyme, and the ligand in the crystal structure of AChE and the re-docked ligand were almost superimposed. The RMSD value between the crystal structure pose and re-docked galantamine pose in active 4EY6 residues was 0.8994 Å (Figure 9). This low RMSD value indicated that the docking procedure was valid, as it was significantly lower than the maximum allowable value of 2.0 Å (Şahin et al., 2022a, 2022b; 2023).

The analysis of the binding orientation of Galantamine showed that Glu202 and Ser203 are important residues that form hydrogen bonds with the reference ligand (Figure 10). This interaction is further stabilized by hydrophobic bonds with Trp86, Gly121, Gly122, Tyr124, Phe295, Phe297, Tyr337, Phe338 and His447. It is worth noting that in previous studies, Trp86, Phe297, Tyr337, Tyr341 and His447 have contributed as being involved in the active site of the AChE enzyme (Begum et al., 2022; Ghosh et al., 2022; Hung et al., 2022).

Synthetic compounds were then docked to the active site pocket of AChE using the same protocol with a galantamine docking condition. The docking analysis results showed that all binding energies of the best-docked poses of the compounds and Galantamine were in the range of −9.1 to −10.3 kcal/mol. According to the results of docking analysis, 9c, which was the most active compound in *in vitro* AChE analysis, was also the most active compound in docking analysis. When looking at the binding energies of the compounds in general, synthetic compounds (in the range −9.9 to −10.3 kcal/mol) showed a more active binding affinity than the reference compound galantamine (−9.1 kcal/mol). The results of molecular docking on AChE are given in Table 7.

All compounds exhibited H-bond interactions with at least one of the critical residues in the active site of the enzyme. These interactions are stabilized by hydrophobic interactions depending on the conformation of the molecule during interaction with the enzyme. When the detailed interaction of 9c, the most active compound, is interpreted, it will be seen that the molecule interacts with six different critical residues. From these residues, H-bond interaction was formed with Phe295. This interaction occurred between the O in the

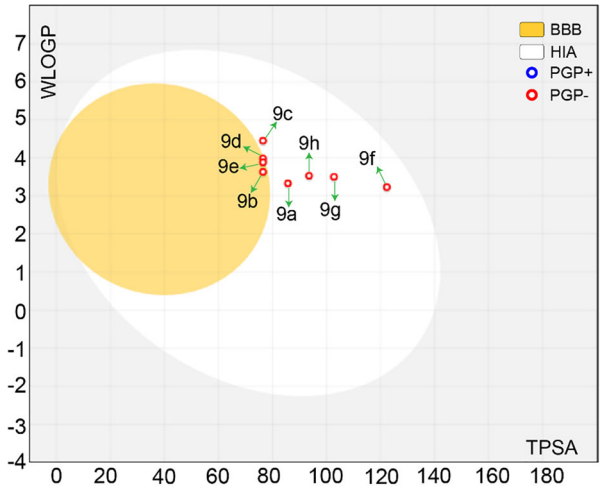

Figure 8. The BOILED-Egg ADME diagram of the compounds (**9a–h**) WLOGP vs. TPSA.

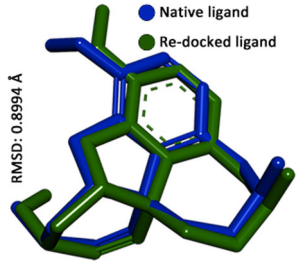

Figure 9. Validation of molecular docking protocol.

Table 6. Toxicity prediction results of compounds.

		Compound							
Properties	Unit	9a	9b	9c	9d	9e	9f	9g	9h
AMES toxicity	Categorical (Yes/No)	No	No	No	No	No	Yes	No	No
Max. tolerated dose (human)	Numeric (log mg/kg/day)	0.253	0.014	0.124	0.022	0.225	−0.158	0.276	0.132
hERG I inhibitor	Categorical (Yes/No)	No	No	No	No	No	No	No	No
hERG II inhibitor	Categorical (Yes/No)	No	No	No	No	No	No	No	No
Oral Rat Acute Toxicity (LD50)	Numeric (mol/kg)	2.282	2.112	2.33	2.192	2.241	2.919	2.302	2.228
Oral Rat Chronic Toxicity (LOAEL)	Numeric (log mg/kg_bw/day)	1.088	1.12	0.937	0.893	1.045	1.012	0.999	1.108
Hepatotoxicity	Categorical (Yes/No)	Yes	Yes	Yes	Yes	Yes	Yes	Yes	Yes
Skin Sensitization	Categorical (Yes/No)	No	No	No	No	No	No	No	No
T.Pyriformis toxicity	Numeric (log µg/L)	0.472	0.68	0.675	0.667	0.48	0.467	0.391	0.515
Minnow toxicity	Numeric (log mM)	−0.908	−0.544	−1.826	−0.762	−0.62	−1.374	−0.453	−0.535

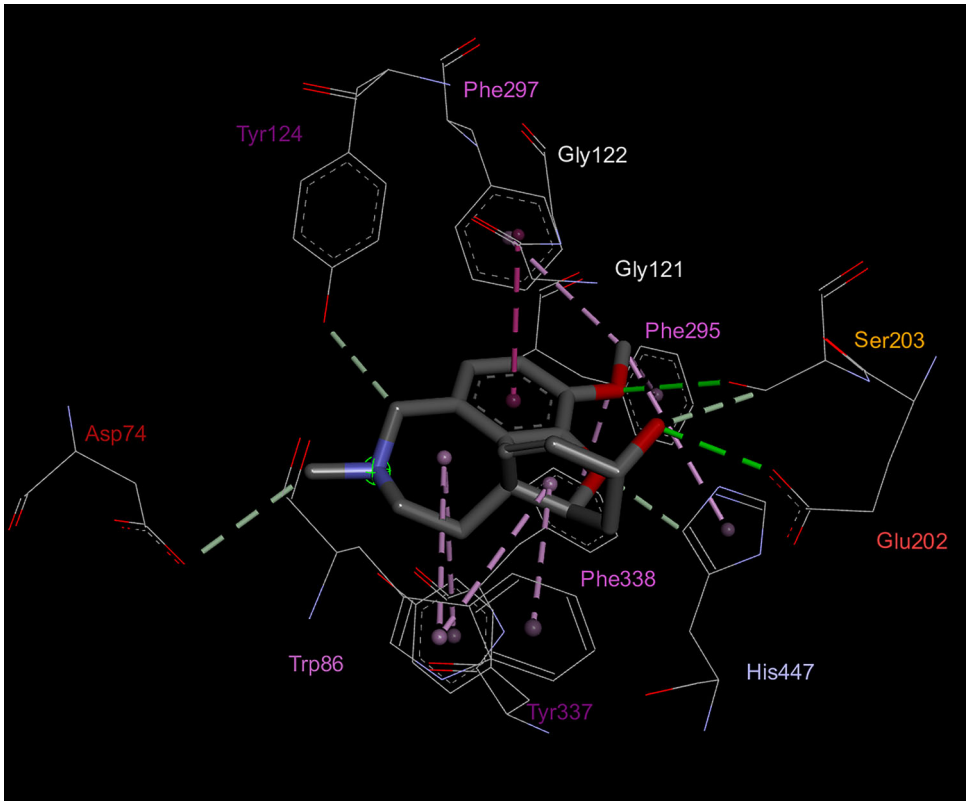

Figure 10. Binding pose of docked native ligand galantamine at the binding site of the AChE enzyme with interacting residues (4EY6).

Table 7. Interaction and amino acid residues involved in the inhibition of AChE enzyme summary.

Comp.	Binding affinity (kcal/mol)	Type of interaction bond	Involved receptor residues
9a	−10.2	HB, C-HB, HP	Trp86, Tyr124, Phe295, Tyr337, Tyr341, His447, Trp286
9b	−10.2	HB, C-HB, HP	Trp86, Asp74, Tyr124, Phe295, Tyr337, Tyr341, His447, Trp286
9c	−10.3	HB, HP	Trp86, Tyr124, Val294, Phe295, Tyr341, His447, Trp286
9d	−9.9	HB, C-HB, HP, HL	Trp86, Asp74, Tyr124, Val294, Phe295, Tyr337, Tyr341, His447, Trp286, Ser293
9e	−10.0	HB, C-HB, HP, HL	Trp86, Asp74, Tyr124, Val294, Phe295, Phe297, Tyr337, Leu130, Tyr341, His447, Trp286, Ser293, Gly120, Gly121, Phe338
9f	−10.0	HP, HB	Trp86, Tyr124, His447, Trp286
9g	−9.9	HB, C-HB, HP	Trp86, Tyr124, Leu289, Tyr337, His447, Trp286
9h	−10.2	HB, C-HB, HP	Trp86, Tyr124, Tyr337, His447, Trp286
GAL	−9.1	HB, C-HB, HP	Trp86, Gly121, Gly122, Tyr124, Phe295, Phe297, Tyr337, Phe338, His447, Glu202, Ser203, Asp74, Trp86

Key: HB:hydrogen bond; C-HB: Carbon-Hydrogen Bond, HP: Hydrophobic interaction, HL: Galogen GAL:Galantamine.

sulfonamide group and the amine group of the residue. Although other interactions are hydrophobic, critic residues with aromatic structures Trp (86 and 286) and Tyr (124, 337 and 341) ensured the molecule's stability in the active site. As in Figure 11, compound 9c key interactions formed T-shaped Pi-Pi between the triazole ring in the molecule and Tyr337, Tyr124 and Tyr 341. These bonds are formed by overlapping the pi orbitals (between the aromatic ring of the residue and the triazole ring) in the residues and the molecule, creating a stable and strong bond. Trp286 residue, on the other hand, interacted with the benzene ring to which the sulfonamide group is attached, through pi–pi stacking, and pi–alkyl interaction with the tosylate methyl group. Pi–pi T-shaped and pi alkyl interactions occurred between Trp86, and the benzene ring attached to the triazole group. Trp86 also exhibited pi-alkyl interaction with the isopropyl group.

4. Conclusions

Eight new hybrid triazole derivatives (**9a–h**) used in this study were synthesized as a result of a series of reactions. The molecular structure of five of the triazole derivatives (**9a–e**) was determined by X-ray diffraction method. DPPH, ABTS·+ and Cuprac methods were used to determine the antioxidant activities of new hybrid triazole derivatives. It was determined

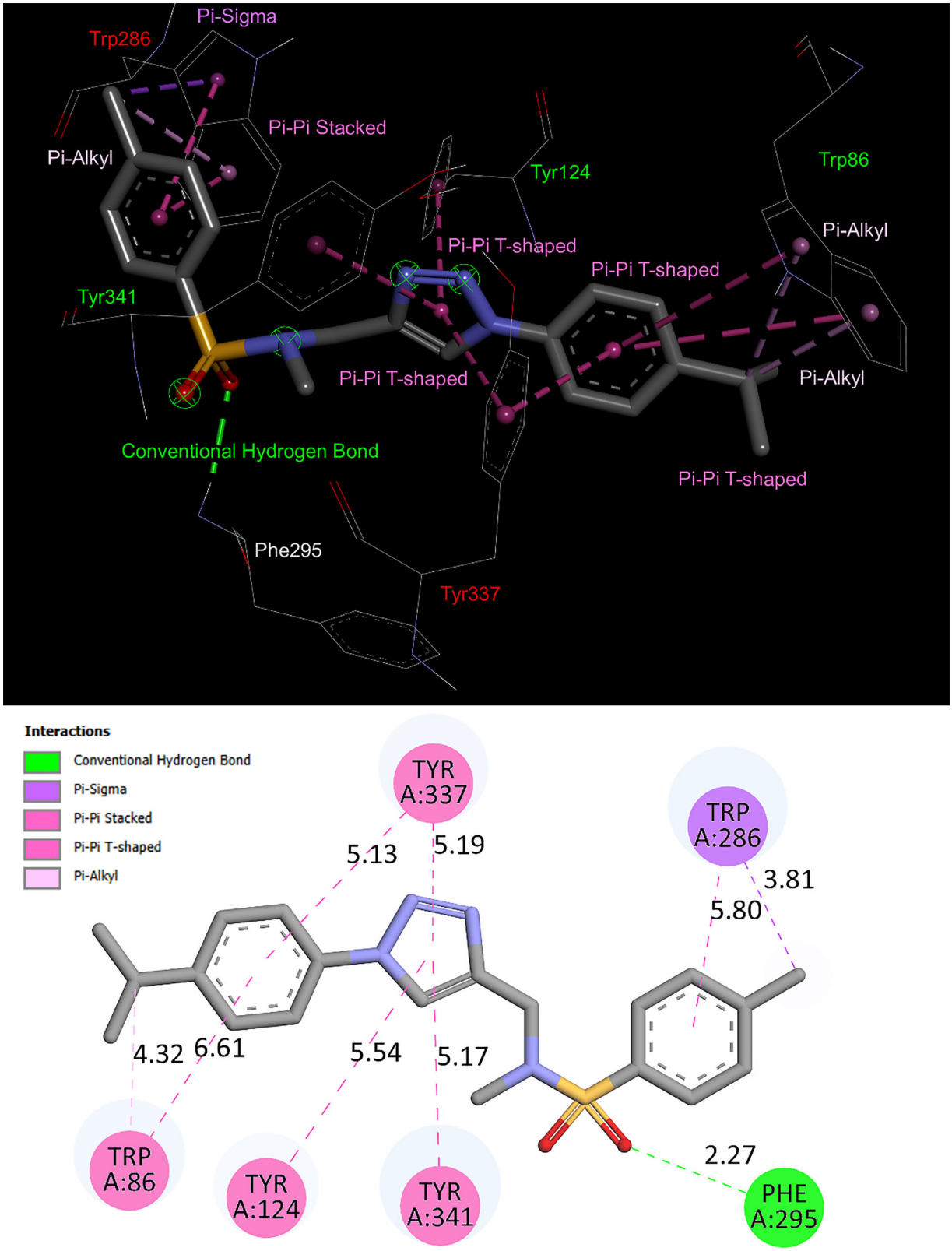

Figure 11. 2D and 3D depiction of **9c** compound which has maximum score with 4EY6.

that all the compounds had various levels of antioxidant activities according to all three methods. It was determined that DPPH activity of two of the synthesized compounds (**9f** and **9h**) was higher than BHT and lower than Ascorbic acid and α-Tacoferol. It was determined that these compounds exhibited radical scavenging activity against ABTS + radicals, which were lower than Ascorbic acid and BHT, and better than α-Tacopherol, except for **9b**. The cytotoxic activities of synthesized compounds (**9a–h**) against A549 and healthy cell line (HDF) were investigated. It can be said that especially the two

hybrid structures (**9d** and **9g**) have excellent both anticancer activity and cytotoxic effect compared to standard *cis*-platin. Two derivatives (**9h** and **9c**) showed moderate anticancer activity, while the others showed less anticancer activity. According to these results, **9d** and **9g** compounds may be anticancer agent candidates. The AChE and BuChE inhibitory properties of the synthesized hybrid structures were investigated and found to have significant values. It was determined that AChE inhibitor activities of all compounds were much better than Galantamine used as standard. In particular, **9c** was found to have ten times better activity than the standard compound. According to the determined BuChE inhibitor properties of the compounds, it was determined that they have better inhibitory activity than **9g** and **9h** Galantamine. The ADMET properties of the molecules have been thoroughly examined and have been found to meet the criteria for drug-like substances. These molecules also have a high rate of oral absorption, as they can effectively cross the blood-brain barrier and are easily absorbed in the gastrointestinal tract. In addition, a molecular docking study was conducted to predict how these compounds may interact with the acetylcholinesterase enzyme.

It can be said that all the hybrid structures synthesized have significant antioxidant, anticancer, cytotoxic, and anti-Alzheimer activities and can be used in further pharmacological studies.

Acknowledgments

This study is dedicated to our esteemed colleague İrfan Şahin and his family, who lost their lives in the earthquake in Kahramanmaraş that occurred on February 6, 2023.

Disclosure Statement

The authors declare no conflict of interest.

Funding

The authors thanks Kahramanmaras Sutcu Imam University Scientific Research Projects Unit (Project code: DOSAP-2021/3-33 D) (Turkey) for funding.

ORCID

İrfan Şahin http://orcid.org/0000-0002-0547-9888
Mustafa Çeşme http://orcid.org/0000-0002-2020-5965
Özge Güngör http://orcid.org/0000-0003-3529-2704
Fatma Betül Özgeriş http://orcid.org/0000-0002-4568-5782
Muhammet Köse http://orcid.org/0000-0002-4597-0858
Ferhan Tümer http://orcid.org/0000-0003-2222-2133

Authors' Contributions

İ.Ş.; investigation, methodology, original draft preparation, writing, M.Ç.; in silico analysis, software, original draft preparation, writing-review, and editing, Ö. G.; enzyme inhibition analysis, F.B.Ö.; *in vitro* analysis, M. K.; X-ray analysis, FT; supervision, conceptualization, project administration, funding acquisition.

References

Şahin, İ., Çeşme, M., Özgeriş, F. B., & Tümer, F. (2023). Triazole based novel molecules as potential therapeutic agents: Synthesis, characterization, biological evaluation, in-silico ADME profiling and molecular docking studies. *Chemico-Biological Interactions*, *370*, 110312. https://doi.org/10.1016/J.CBI.2022.110312

Şahin, İ., Çeşme, M., Yüce, N., & Tümer, F. (2022b). Discovery of new 1,4-disubstituted 1,2,3-triazoles: In silico ADME profiling, molecular docking and biological evaluation studies. *Journal of Biomolecular Structure and Dynamics*, *41*(5), 1988–2001. https://doi.org/10.1080/07391102.2022.2025905

Şahin, İ., Özgeriş, F. B., Köse, M., Bakan, E., & Tümer, F. (2021). Synthesis, characterization, and antioxidant and anticancer activity of 1,4-disubstituted 1,2,3-triazoles. *Journal of Molecular Structure*, *1232*, 130042. https://doi.org/10.1016/j.molstruc.2021.130042

Anand, P., & Singh, B. (2013). A review on cholinesterase inhibitors for Alzheimer's disease. *Archives of Pharmacal Research*, *36*(4), 375–399. https://doi.org/10.1007/S12272-013-0036-3

Aziz Ali, A. (2021). 1,2,3-Triazoles: Synthesis and biological application. In *Azoles - synthesis, properties, applications and perspectives* (vol. i, p.13). IntechOpen. https://doi.org/10.5772/intechopen.92692

Bag, S., Tulsan, R., Sood, A., Cho, H., Redjeb, H., Zhou, W., Levine, H., Török, B., & Török, M. (2015). Sulfonamides as multifunctional agents for Alzheimer's disease. *Bioorganic & Medicinal Chemistry Letters*, *25*(3), 626–630. https://doi.org/10.1016/J.BMCL.2014.12.006

Begum, F., Rehman, N. U., Khan, A., Iqbal, S., Paracha, R. Z., Uddin, J., Al-Harrasi, A., & Lodhi, M. A. (2022). 2-Mercaptobenzimidazole clubbed hydrazone for Alzheimer's therapy: In vitro, kinetic, in silico, and in vivo potentials. *Frontiers in Pharmacology*, *13*, 946134. https://doi.org/10.3389/fphar.2022.946134

Bonandi, E., Christodoulou, M. S., Fumagalli, G., Perdicchia, D., Rastelli, G., & Passarella, D. (2017). The 1,2,3-triazole ring as a bioisostere in medicinal chemistry. *Drug Discovery Today*, *22*(10), 1572–1581. https://doi.org/10.1016/j.drudis.2017.05.014

Bozorov, K., Zhao, J., & Aisa, H. A. (2019). 1,2,3-Triazole-containing hybrids as leads in medicinal chemistry: A recent overview. *Bioorganic & Medicinal Chemistry*, *27*(16), 3511–3531. https://doi.org/10.1016/j.bmc.2019.07.005

Casini, A., Scozzafava, A., Mastrolorenzo, A., & Supuran, C. (2002). Sulfonamides and sulfonylated derivatives as anticancer agents. *Current Cancer Drug Targets*, *2*(1), 55–75. https://doi.org/10.2174/1568009023334060

Çeşme, M. (2023). 2-Aminophenol-based ligands and Cu(II) complexes: Synthesis, characterization, X-ray structure, thermal and electrochemical properties, and in vitro biological evaluation, ADMET study and molecular docking simulation. *Journal of Molecular Structure*, *1271*, 134073. https://doi.org/10.1016/j.molstruc.2022.134073

Çot, A., Betül Özgeriş, F., Şahin, İ., Çeşme, M., Onur, S., & Tümer, F. (2022). Synthesis, characterization, antioxidant and anticancer activity of new hybrid structures based on diarylmethanol and 1,2,3-triazole. *Journal of Molecular Structure*, *1269*, 133763. https://doi.org/10.1016/j.molstruc.2022.133763

Çot, A., Çeşme, M., Onur, S., Aksakal, E., Şahin, İ., & Tümer, F. (2022). Rational design of 1,2,3-triazole hybrid structures as novel anticancer agents: Synthesis, biological evaluation and molecular docking studies. *Journal of Biomolecular Structure and Dynamics*, 1–9. https://doi.org/10.1080/07391102.2022.2112620

Cunha, A. C., Jordão, A. K., de Souza, M. C. B. V., Ferreira, V. F., de Almeida, M. C. B., Wardell, J. L., & Tiekink, E. R. T. (2016). 1-Anilino-5-methyl-1 H -1,2,3-triazole-4-carbaldehyde. *IUCrData*, *1*(1), x160038. https://doi.org/10.1107/S2414314616000389/ZQ4001ISUP3.CML

Daina, A., & Zoete, V. (2016). A boiled-egg to predict gastrointestinal absorption and brain penetration of small molecules. *ChemMedChem*, *11*(11), 1117–1121. https://doi.org/10.1002/cmdc.201600182

Daina, A., Michielin, O., & Zoete, V. (2017). SwissADME: A free web tool to evaluate pharmacokinetics, drug-likeness and medicinal chemistry friendliness of small molecules. *Scientific Reports*, *7*(1), 42717. https://doi.org/10.1038/srep42717

Dalvie, D. K., Kalgutkar, A. S., Khojasteh-Bakht, S. C., Obach, R. S., & O'Donnell, J. P. (2002). Biotransformation reactions of five-membered aromatic heterocyclic rings. *Chemical Research in Toxicology*, *15*(3), 269–299. https://doi.org/10.1021/tx015574b

Davis, T. (1976). Selective loss of central cholinergic neurons in Alzheimer's disease. *Lancet*, *2*(8000),1403. https://doi.org/10.1016/s0140-6736(76)91936-x

De Nisi, A., Bergamini, C., Leonzio, M., Sartor, G., Fato, R., Naldi, M., Monari, M., Calonghi, N., & Bandini, M. (2016). Synthesis, cytotoxicity and anti-cancer activity of new alkynyl-gold(i) complexes. *Dalton Transactions (Cambridge, England : 2003)*, *45*(4), 1546–1553. https://doi.org/10.1039/C5DT02905H

Duan, Y. C., Zheng, Y. C., Li, X. C., Wang, M. M., Ye, X. W., Guan, Y. Y., Liu, G. Z., Zheng, J. X., & Liu, H. M. (2013). Design, synthesis and antiproliferative activity studies of novel 1,2,3-triazole-dithiocarbamate-urea hybrids. *European Journal of Medicinal Chemistry*, *64*, 99–110. https://doi.org/10.1016/j.ejmech.2013.03.058

Eggler, J. F. (1995). Benzisothiazoles derivatives as inhibitors of 5-lipoxygenase biosynthesis.

Genç, Y., Özkanca, R., & Bekdemir, Y. (2008). Antimicrobial activity of some sulfonamide derivatives on clinical isolates of Staphylococus aureus. *Annals of Clinical Microbiology and Antimicrobials*, *7*, 17. https://doi.org/10.1186/1476-0711-7-17

Ghosh, S., Jana, K., Wakchaure, P. D., & Ganguly, B. (2022). Revealing the cholinergic inhibition mechanism of Alzheimer's by galantamine: A metadynamics simulation study. *Journal of Biomolecular Structure & Dynamics*, *40*(11), 5100–5111. https://doi.org/10.1080/07391102.2020.1867644/SUPPL_FILE/TBSD_A_1867644_SM7098.PDF

Giacobini, E. (2001). Selective inhibitors of butyrylcholinesterase: A valid alternative for therapy of Alzheimer's disease? *Drugs & Aging*, *18*(12), 891–898. https://doi.org/10.2165/00002512-200118120-00001

Giacobini, E. (2004). Cholinesterase inhibitors: New roles and therapeutic alternatives. *Pharmacological Research*, *50*(4), 433–440. https://doi.org/10.1016/J.PHRS.2003.11.017

Hamedi, A., Zengin, G., Aktumsek, A., Selamoglu, Z., & Pasdaran, A. (2020). In vitro and in silico approach to determine neuroprotective properties of iridoid glycosides from aerial parts of Scrophularia amplexicaulis by investigating their cholinesterase inhibition and antioxidant activities. *Biointerface Research in Applied Chemistry*, *10*(3), 5429–5454. https://doi.org/10.33263/BRIAC103.429454

Horne, W. S., Yadav, M. K., Stout, C. D., & Ghadiri, M. R. (2004). Heterocyclic peptide backbone modifications in an r-helical coiled coil. *Journal of the American Chemical Society*, *126*(47), 15366–15367. https://doi.org/10.1021/ja0450408

Hung, N. H., Quan, P., Satyal, M., Dai, P., Hoa, D. N., van, V., Huy, N. G., Giang, L. D., Ha, N. T., Huong, L. T., Hien, V. T., & Setzer, W. N. (2022). Acetylcholinesterase inhibitory activities of essential oils from vietnamese traditional medicinal plants. *Molecules*, *27*(20), 7092. https://doi.org/10.3390/molecules27207092

Isika, D. K., Özkömeç, F. N., Çeşme, M., & Sadik, O. A. (2022). Synthesis, biological and computational studies of flavonoid acetamide derivatives. *RSC Advances*, *12*(16), 10037–10050. https://doi.org/10.1039/d2ra01375d

Kamal, A., Shankaraiah, N., Devaiah, V., Laxma Reddy, K., Juvekar, A., Sen, S., Kurian, N., & Zingde, S. (2008). Synthesis of 1,2,3-triazole-linked pyrrolobenzodiazepine conjugates employing "click" chemistry: DNA-binding affinity and anticancer activity. *Bioorganic & Medicinal Chemistry Letters*, *18*(4), 1468–1473. https://doi.org/10.1016/j.bmcl.2007.12.063

Kar, S., & Leszczynski, J. (2020). Open access in silico tools to predict the ADMET profiling of drug candidates. *Expert Opinion on Drug Discovery*, *15*(12), 1473–1487. https://doi.org/10.1080/17460441.2020.1798926

Khalid, S., Zahid, M. A., Ali, H., Kim, Y. S., & Khan, S. (2018). Biaryl scaffold-focused virtual screening for anti-aggregatory and neuroprotective effects in Alzheimer's disease. *BMC Neuroscience*, *19*(1), 74. https://doi.org/10.1186/s12868-018-0472-6

Köksal, Z., Alım, Z., Bayrak, S., Gülçin, İ., & Özdemir, H. (2019). Investigation of the effects of some sulfonamides on acetylcholinesterase and carbonic anhydrase enzymes. *Journal of Biochemical and Molecular Toxicology*, *33*(5), e22300. https://doi.org/10.1002/jbt.22300

Kołaczek, A., Fusiarz, I., Ławecka, J., & Branowska, D. (2014). Biological activity and synthesis of sulfonamide derivatives: A brief review. *Chemik*, *68*, 620–628.

Kung, H. F., Lee, C. W., Zhuang, Z. P., Kung, M. P., Hou, C., & Plössl, K. (2001). Novel stilbenes as probes for amyloid plaques. *Journal of the American Chemical Society*, *123*(50), 12740–12741. https://doi.org/10.1021/JA0167147/SUPPL_FILE/JA0167147_S2.PDF

Lipinski, C. A. (2004). Lead- and drug-like compounds: The rule-of-five revolution. *Drug Discovery Today. Technologies*, *1*(4), 337–341. https://doi.org/10.1016/j.ddtec.2004.11.007

Liu, C. J., Liu, Y. P., Yu, S. L., Dai, X. J., Zhang, T., & Tao, J. C. (2016). Syntheses, cytotoxic activity evaluation and HQSAR study of 1,2,3-triazole-linked isosteviol derivatives as potential anticancer agents. *Bioorganic & Medicinal Chemistry Letters*, *26*(22), 5455–5461. https://doi.org/10.1016/j.bmcl.2016.10.028

Luo, W., Chen, Y., Wang, T., Hong, C., Chang, L. P., Chang, C. C., Yang, Y. C., Xie, S. Q., & Wang, C. J. (2016). Design, synthesis and evaluation of novel 7-aminoalkyl-substituted flavonoid derivatives with improved cholinesterase inhibitory activities. *Bioorganic & Medicinal Chemistry*, *24*(4), 672–680. https://doi.org/10.1016/j.bmc.2015.12.031

Makarian, M., Gonzalez, M., Salvador, S. M., Lorzadeh, S., Hudson, P. K., & Pecic, S. (2022). Synthesis, kinetic evaluation and molecular docking studies of donepezil-based acetylcholinesterase inhibitors HHS Public Access. *Journal of Molecular Structure*. *1247*, 131425. https://doi.org/10.1016/j.molstruc.2021.131425

Malani, A. H., Makwana, A. H., & Makwana, H. (2017). A brief review article: Various synthesis and therapeutic importance of 1,2,4-triazole and its derivatives. *Moroccan Journal of Chemistry*, *5*(1), 41–58.

Martin Prince, A., Wimo, A., Guerchet, M., Gemma-Claire Ali, M., Wu, Y.-T., Prina, M., Yee Chan, K., & Xia, Z. (2015). *World Alzheimer Report 2015 The Global Impact of Dementia An AnAlysIs of prevAlence, InclDence, cosT AnD TrenDs*. www.alz.co.uk/worldreport2015corrections.

Orhan, I. E., Senol Deniz, F. S., Traedal-Henden, S., Cerón-Carrasco, J. P., den Haan, H., Peña-García, J., Pérez-Sánchez, H., Emerce, E., & Skalicka-Wozniak, K. (2019). Profiling auspicious butyrylcholinesterase inhibitory activity of two herbal molecules: Hyperforin and Hyuganin C. *Chemistry & Biodiversity*, *16*(5), e1900017. https://doi.org/10.1002/CBDV.201900017

Penthala, N. R., Madhukuri, L., Thakkar, S., Madadi, N. R., Lamture, G., Eoff, R. L., & Crooks, P. A. (2015). Synthesis and anti-cancer screening of novel heterocyclic-(2H)- 1,2,3-triazoles as potential anti-cancer agents. *MedChemComm*, *6*(8), 1535–1543. https://doi.org/10.1039/C5MD00219B

Perlovich, G. L., Ryzhakov, A. M., Tkachev, V. V., Hansen, L. K., & Raevsky, O. A. (2013). Sulfonamide molecular crystals: Structure, sublimation thermodynamic characteristics, molecular packing, hydrogen bonds networks. *Crystal Growth & Design*, *13*(9), 4002–4016. https://doi.org/10.1021/cg400666v

Pires, D. E. V., Blundell, T. L., & Ascher, D. B. (2015). pkCSM: Predicting small-molecule pharmacokinetic and toxicity properties using graph-based signatures. *Journal of Medicinal Chemistry*, *58*(9), 4066–4072. https://doi.org/10.1021/acs.jmedchem.5b00104

Raina, P., Santaguida, P., Ismaila, A., Patterson, C., Cowan, D., Levine, M., Booker, L., & Oremus, M. (2008). Effectiveness of cholinesterase inhibitors and memantine for treating dementia: Evidence review for a clinical practice guideline. *Annals of Internal Medicine*, *148*(5), 379–397. https://doi.org/10.7326/0003-4819-148-5-200803040-00009

Reedijk, J. (1996). Improved understanding in platinium antitumour chemistry. *Chemical Communications*, *7*(7), 801. https://doi.org/10.1039/cc9960000801

Şahin, İ., Çeşme, M., Özgeriş, F. B., Güngör, Ö., & Tümer, F. (2022a). Design and synthesis of 1,4-disubstituted 1,2,3-triazoles: Biological evaluation, in silico molecular docking and ADME screening. *Journal of Molecular Structure*, *1247*, 131344. https://doi.org/10.1016/j.molstruc.2021.131344

Santos, M. A., Marques, S. M., Tuccinardi, T., Carelli, P., Panelli, L., & Rossello, A. (2006). Design, synthesis and molecular modeling study

of iminodiacetyl monohydroxamic acid derivatives as MMP inhibitors. *Bioorganic & Medicinal Chemistry*, *14*(22), 7539–7550. https://doi.org/10.1016/j.bmc.2006.07.011

Singla, S., & Piplani, P. (2016). Coumarin derivatives as potential inhibitors of acetylcholinesterase: Synthesis, molecular docking and biological studies. *Bioorganic & Medicinal Chemistry*, *24*(19), 4587–4599. https://doi.org/10.1016/j.bmc.2016.07.061

Stefely, J. A., Palchaudhuri, R., Miller, P. A., Peterson, R. J., Moraski, G. C., Hergenrother, P. J., & Miller, M. J. (2010). N -((1-benzyl-1 H -1,2,3-triazol-4-yl)methyl)arylamide as a new scaffold that provides rapid access to antimicrotubule agents: Synthesis and evaluation of antiproliferative activity against select cancer cell lines. *Journal of Medicinal Chemistry*, *53*(8), 3389–3395. https://doi.org/10.1021/jm1000979

Turkan, F., Cetin, A., Taslimi, P., & Gulçin, İ. (2018). Some pyrazoles derivatives: Potent carbonic anhydrase, α-glycosidase, and cholinesterase enzymes inhibitors. *Archiv der Pharmazie*, *351*(10), 1800200. (https://doi.org/10.1002/ardp.201800200

Wan, H. (2013). What ADME tests should be conducted for preclinical studies? *ADMET & DMPK*, *1*(3), 19–28. https://doi.org/10.5599/admet.1.3.9

Yeşilkaynak, T., Özkömeç, F. N., Çeşme, M., Demirdöğen, R. E., Kutlu, E., Kutlu, H. M., & Emen, F. M. (2022). Synthesis of new thiourea derivatives and metal complexes: Thermal behavior, biological evaluation, in silico ADMET profiling and molecular docking studies. *Journal of Molecular Structure*, *1269*, 133758. https://doi.org/10.1016/j.molstruc.2022.133758